


Review

# Recent Advances in Vanadium-Based Electrocatalysts for Hydrogen and Oxygen Evolution Reactions: A Review

Haoyu Li<sup>1</sup>, Juan Wu<sup>1</sup>, Mengyao Li<sup>1</sup> and Yude Wang<sup>2,\*</sup> 

<sup>1</sup> National Center for International Research on Photoelectric and Energy Materials, School of Materials and Energy, Yunnan University, Kunming 650504, China; lhy2022tj@mail.ynu.edu.cn (H.L.); wujuan1@stu.ynu.edu.cn (J.W.); myli@mail.ynu.edu.cn (M.L.)

<sup>2</sup> Yunnan Key Laboratory of Carbon Neutrality and Green Low-Carbon Technologies, Yunnan University, Kunming 650504, China

\* Correspondence: ydwang@ynu.edu.cn

**Abstract:** With the intensification of global resource shortages and the environmental crisis, hydrogen energy has garnered significant attention as a renewable and clean energy source. Water splitting is considered the most promising method of hydrogen production due to its non-polluting nature and high hydrogen concentration. However, the slow kinetics of the two key reactions, the Hydrogen Evolution Reaction (HER) and Oxygen Evolution Reaction (OER), have greatly limited the development of related technologies. Meanwhile, the scarcity and high cost of precious metal catalysts represented by Pt and Ir/RuO<sub>2</sub> limit their large-scale commercial application. Thus, it is essential to develop catalysts based on Earth's transition metals that have abundant reserves. Vanadium (V) is an early transition metal with a distinct electronic structure from late transition metals such as Fe, Co, and Ni, which has been emphasized and studied by researchers. Numerous vanadium-based electrocatalysts have been developed for the HER and OER. In this review, the mechanisms of the HER and OER are described. Then, the compositions, properties, and modification strategies of various vanadium-based electrocatalysts are summarized, which include vanadium-based oxides, hydroxides, dichalcogenides, phosphides, nitrides, carbides, and vanadate. Finally, potential challenges and future perspectives are presented based on the current status of V-based electrocatalysts for water splitting.

**Keywords:** vanadium based; electrocatalysts; HER; OER



**Citation:** Li, H.; Wu, J.; Li, M.; Wang, Y. Recent Advances in Vanadium-Based Electrocatalysts for Hydrogen and Oxygen Evolution Reactions: A Review. *Catalysts* **2024**, *14*, 368. <https://doi.org/10.3390/catal14060368>

Academic Editor: Zuzeng Qin

Received: 16 April 2024

Revised: 2 June 2024

Accepted: 3 June 2024

Published: 5 June 2024



**Copyright:** © 2024 by the authors. Licensee MDPI, Basel, Switzerland. This article is an open access article distributed under the terms and conditions of the Creative Commons Attribution (CC BY) license (<https://creativecommons.org/licenses/by/4.0/>).

## 1. Introduction

With the increasing global demand for energy and the urgent need to reduce greenhouse gas emissions, it is urgent to develop clean and renewable energy solutions [1–3]. Hydrogen is a promising energy carrier due to its high energy density and only releasing water when burned [4–6]. Among many technologies for hydrogen production, electrocatalytic water splitting is an efficient and environmentally friendly approach [7–10]. However, the slow kinetics of the HER and OER limit the wide application of electrocatalytic hydrogen production. Utilizing high-efficiency electrocatalysts can decrease the energy barrier and accelerate the reaction kinetics in water electrolysis, resulting in reduced energy usage [11–13]. The prevailing catalysts employed for electrocatalytic hydrogen production in the industry are commonly platinum group catalysts, specifically Pt/C and Ir/RuO<sub>2</sub>. Nevertheless, their high cost and scarcity pose major challenges for large-scale applications [14–17]. Consequently, it is critical to create electrocatalysts based on transition metals. These catalysts should perform well in the actual production process, be cost-effective, and have sufficient reserves [18–21].

Vanadium, as an early transition metal element, possesses a wide range of oxidation states. This characteristic offers numerous possibilities for adjusting the electronic structure

of materials, hence enhancing their catalytic performances [22–24]. Vanadium-based catalysts are a viable alternative to replace scarce and costly noble metals in water splitting due to their adaptable redox chemistry and plentiful availability at affordable prices on Earth [25–28]. Angnes et al. presented a comprehensive summary of the progress of NiV-LDHs as electrocatalysts for water splitting, pointing out that NiV-LDHs have significant potential in the HER and OER [29]. Yang et al. synthesized ternary  $\text{Co}_{1-x}\text{V}_x\text{P}$  nanoneedle arrays by hydrothermal low-temperature phosphorization. In 1 M KOH, the nanoneedle arrays demonstrated current densities of 10 and 400  $\text{mA cm}^{-2}$ , with corresponding overpotential values of 46 and 226 mV, respectively. In addition, the current densities of 10, 100, and 300  $\text{mA cm}^{-2}$  were achieved at voltages of 1.58, 1.75, and 1.92 V, respectively. when  $\text{Co}_{1-x}\text{V}_x\text{-HNNs}$  were utilized as the anode and  $\text{Co}_{1-x}\text{V}_x\text{P}$  as the cathode in a device for overall water splitting [30].

In this review, we comprehensively summarize the compositions, properties, and modification strategies of vanadium-based electrocatalysts, including oxides, hydroxides, phosphides, carbides, nitrides, dichalcogenides, and vanadates (Figure 1). Additionally, we present tables to summarize the activity, stability, and preparation methods of representative vanadium-based electrocatalysts. In conclusion, we highlight the existing issues with vanadium-based electrocatalysts for water splitting and propose recommendations to promote the development of V-based electrocatalysts for the HER and OER.

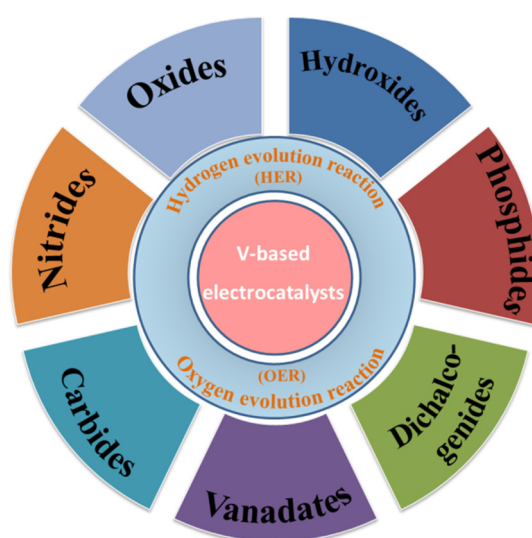


**Figure 1.** Schematic organization of the vanadium-based electrocatalysts including oxides, hydroxide, phosphides, dichalcogenides, vanadates, carbides, and nitrides with the HER and OER.

## 2. Fundamentals of the HER and OER

As shown in Figure 2A, water splitting consists of two key half-reactions (the HER for the cathode and OER for the anode). The thermodynamic theoretical voltage of water splitting is 1.23 V. However, an additional potential is dissipated for water splitting due to the slow reaction kinetics of the HER and OER, which is called overpotential ( $\eta$ ). Therefore, the actual voltages of water splitting ( $E$ ) are shown in Equation (1) as follows.

$$E = 1.23 \text{ V} + \eta_{\text{HER}} + \eta_{\text{OER}} + iR \quad (1)$$

$iR$  is the ohmic potential drop of the system. From Equation (1), it can be seen that the focus of reducing the voltage of water splitting is to develop efficient electrocatalysts to reduce  $\eta_{\text{HER}}$  and  $\eta_{\text{OER}}$  [29].

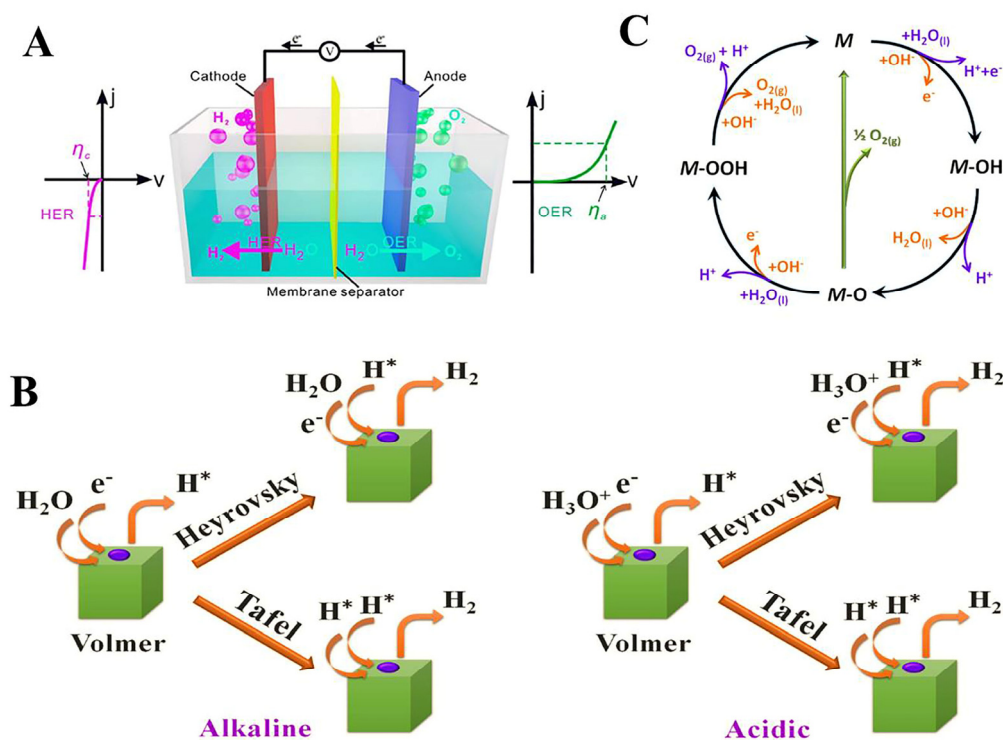


**Figure 2.** (A) Schematic illustration of water splitting. Reproduced with permission [29]. Copyright 2021 Elsevier. (B) Scheme of the possible reaction steps of the OER under acidic (purple lines) and alkaline conditions (orange lines). (C) Scheme of the possible reaction steps of the OER under acidic and alkaline conditions. Reproduced with permission [31]. Copyright 2022 Elsevier.

### 2.1. Mechanism of the HER

The HER is a two-electron transfer reduction reaction involving the adsorption and desorption of H intermediates ( $H^*$ ). The difference in electrolyte pH affects the source of protons (mainly from  $H_2O$  under alkaline conditions and from  $H^+$  under acidic conditions). Therefore, the hydrogen production mechanism is different in acidic and basic conditions [31].

#### 2.1.1. Reaction Mechanism of the HER under Acidic Conditions

Volmer reaction (electrochemical adsorption):



Heyrovsky reaction (electrochemical desorption):



Tafel reaction (chemical desorption):



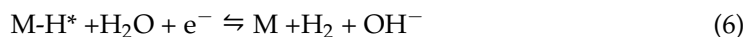
A large amount of  $H^+$  is present in acidic conditions. Initially, the  $H^+$  ions adhere to the surface of the catalyst and create  $M-H^*$  (where  $H^*$  represents the attachment of hydrogen atoms to the active site  $M$  on the catalyst surface), which is known as the Volmer reaction (Equation (2)). The subsequent desorption step may be electrochemical desorption (Equation (3)) or chemical desorption (Equation (4)) depending on the nature of the electrocatalyst (Figure 2B).

### 2.1.2. Reaction Mechanism of the HER under Alkaline Conditions

Volmer reaction (electrochemical adsorption):



Heyrovsky reaction (electrochemical desorption):



Tafel reaction (chemical desorption):

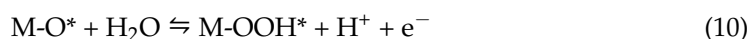
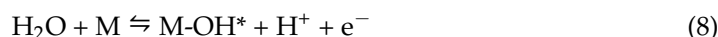


The process of the HER in alkaline solutions is analogous to that in acidic solutions. It involves the Volmer reaction (Equation (5)), Heyrovsky reaction (Equation (6)), and Tafel reaction (Equation (7)). However, due to the minimal concentration of  $\text{H}^+$  in alkaline solutions, the process of water molecule dissociation is necessary to acquire  $\text{H}^+$ . Consequently, the HER kinetics of electrocatalysts in an alkaline environment are significantly slower than that of an acidic environment.

### 2.2. Mechanism of the OER

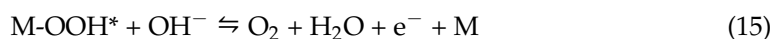
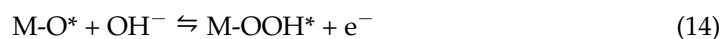
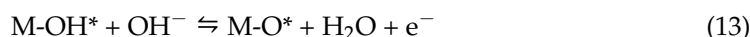
The OER is a four-electron transfer process that occurs at the anode in water splitting. Similar to the HER, the mechanism of the OER is different in acidic and alkaline solutions [31].

#### 2.2.1. Reaction Mechanism of the OER under Acidic Conditions



Water molecules are required to dissociate  $\text{OH}^-$  under acidic conditions because trace amounts of  $\text{OH}^-$  are present in acidic solutions (Figure 2C). Initially,  $\text{OH}^-$  attaches to the catalyst surface to generate  $\text{M-OH}^*$  (Equation (8)), which is subsequently deprotonated to form  $\text{M-O}^*$  (Equation (9)), and  $\text{M-O}^*$  is attacked by the nucleophilic attack of water molecules to generate  $\text{M-OOH}^*$  (Equation (10)) and finally further oxidized to release oxygen (Equation (11)).

#### 2.2.2. Reaction Mechanism of the OER under Alkaline Conditions



The process of the OER in alkaline solutions is analogous to that in acidic solutions. It involves the generation of intermediates such as  $\text{OH}^*$ ,  $\text{O}^*$ , and  $\text{OOH}^*$ . Considering that the OER is an oxidation reaction, metals prone to high valence valorization are beneficial for enhancing the performance of the OER [32,33].

### 3. Vanadium-Based Electrocatalysts for the HER and OER

#### 3.1. Vanadium-Based Oxides

Benefiting from the fact that V has different valence states, vanadium-based oxides have adjustable valence states, which provides more options and flexibility for the design and optimization of electrocatalysts for water splitting [34,35]. Nevertheless, improving the electrocatalytic efficiency of V-based oxides is still a significant obstacle due to the low intrinsic conductivity of the oxides [36]. Presently, the most widely used vanadium-based oxide systems include  $\text{V}_2\text{O}_3$ ,  $\text{VO}_2$ , and  $\text{V}_2\text{O}_5$ . Their performance in terms of the HER and OER, as well as the modification strategies, are summarized here.

##### 3.1.1. HER Performance

V-based oxides typically exhibit semiconductor behavior, and their inadequate electrical conductivity hampers their HER performance. Presently, the main modification approach is to compound transition metal monomers or alloys with V-based oxides. This has two benefits: firstly, it enhances the electrical conductivity of V-based oxides, and secondly, it takes advantage of the strong affinity of  $\text{VO}_x$  for oxygen. This affinity allows  $\text{VO}_x$  to act as a center for dissociating water molecules, thereby improving the kinetics of the HER [37,38]. Li et al. successfully synthesized  $\text{NiCo}/\text{V}_2\text{O}_3/\text{C}$  by hydrothermal and thermal reduction. On the one hand, a Mott–Schottky junction was formed between the NiCo alloy and  $\text{V}_2\text{O}_3$  (Figure 3A,B), which enhanced the charge transfer rate, and the HER activity was significantly increased. In addition, the graphite phase carbon layer acts as a support for the heterostructure, which greatly improves the stability of the material during the HER. Meanwhile, DFT calculations showed that the heterogeneous interface optimized both the hydrogen adsorption free energy and  $\text{H}_2\text{O}$  adsorption energy, which promoted the HER kinetics (Figure 3C) [39].

Utilizing crystalline phase engineering is an effective method for enhancing the efficiency of electrocatalysts.  $\text{VO}_2$  exhibits several crystalline forms, such as  $\text{VO}_2$  (A) and  $\text{VO}_2$  (R) with tetragonal structures, and  $\text{VO}_2$  (B) and  $\text{VO}_2$  ( $\text{M}_1$ ) with monoclinic structures [40]. Although their chemical composition is identical, there are notable distinctions in their optoelectronic characteristics. The reason for this is that the insulator  $\text{VO}_2$  ( $\text{M}_1$ ), which has a monoclinic structure, converts into the metallic phase  $\text{VO}_2$  (R) with a rutile structure by insulator-to-metal transition (IMT). This transition causes a substantial decrease in the resistivity of the material [41]. Kim et al. successfully applied the IMT of  $\text{VO}_2$  to the electrocatalytic field. Firstly,  $\text{VO}_2$  ( $\text{M}_1$ ) was successfully synthesized by hydrothermal and solid-phase sintering methods. As shown in Figure 4A,B, DSC and in situ XRD verified that  $\text{VO}_2$  ( $\text{M}_1$ ) was induced to be converted to  $\text{VO}_2$  (R) by a homemade electrode-heating system. The overpotential of the HER ( $\eta_{10}$ ) was reduced from 411 mV to 136 mV in 0.5 M  $\text{H}_2\text{SO}_4$ . The significant improvement in the HER performance was attributed to the increase in the ECSA induced by the transformation of the insulator's  $\text{VO}_2$  into metal-phase  $\text{VO}_2$ , as well as the decrease in the charge transfer resistance [42]. Given that the IMT effect in  $\text{VO}_2$  occurs at 68 °C, it aligns with the temperatures achievable under industrial water electrolysis conditions (60–80 °C). Consequently, there is promising potential to further investigate  $\text{VO}_2$  as a water-splitting electrocatalyst.

Due to its inherent difficulty in adsorbing hydrogen and its limited electrical conductivity, the HER performance of pure  $\text{V}_2\text{O}_5$  is not ideal. Currently,  $\text{V}_2\text{O}_5$  is mainly complexed with metal sulfides to promote the dissociation of water molecules through the strong electrostatic attraction generated by its own  $\text{V}^{5+}$ , which in turn improves electrocatalytic activity [43]. Zhong and colleagues utilized a two-step hydrothermal method to cultivate  $\text{V}_2\text{O}_5$  on the surface of  $\text{Ni}_2\text{S}_3$ . The  $\text{V}^{5+}$  species at the  $\text{V}_2\text{O}_5/\text{Ni}_2\text{S}_3$  interface exhibited a

strong electrostatic affinity, allowing them to selectively absorb  $\text{OH}^-$  ions from the electrolyte. The presence of  $\text{Ni}_3\text{S}_2$  at the interface enhances the adsorption of H and speeds up the Volmer process, hence enhancing the electrocatalytic kinetics of the HER [44]. Species with a valence of  $\text{V}^{5+}$  in  $\text{V}_2\text{O}_5$  can hinder the oxidation of metal sulfides by selectively binding with oxygen ( $\text{O}_2$ ). Wu et al. successfully applied  $\text{V}_2\text{O}_5$  colloidal nanoclusters onto  $\text{CoS}_2$ , resulting in a significant decrease in the surface oxidation of  $\text{CoS}_2$  and an enhanced dissociation of water molecules [45]. The HER performance of representative V-based oxides are listed in Table 1.

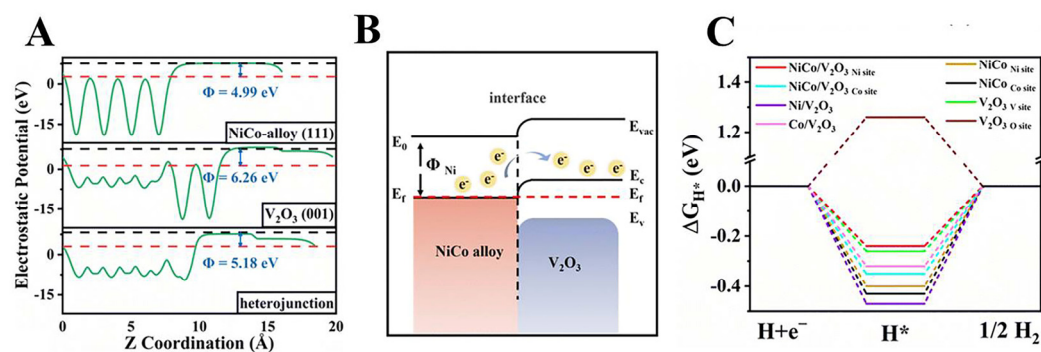


**Figure 3.** (A) The electrostatic potential for NiCo (111),  $\text{V}_2\text{O}_3$  (001), and the Mott–Schottky heterojunction formed from NiCo (111) and  $\text{V}_2\text{O}_3$  (001). (B) Energy band diagram of Ni and  $\text{V}_2\text{O}_3$  with the Mott–Schottky interface after Schottky contact. (C) The hydrogen adsorption Gibbs free energy diagrams of NiCo/ $\text{V}_2\text{O}_3$ , Ni/ $\text{V}_2\text{O}_3$ , Co/ $\text{V}_2\text{O}_3$ , and  $\text{V}_2\text{O}_3$ . Reproduced with permission [39]. Copyright 2023 Royal Society of Chemistry.

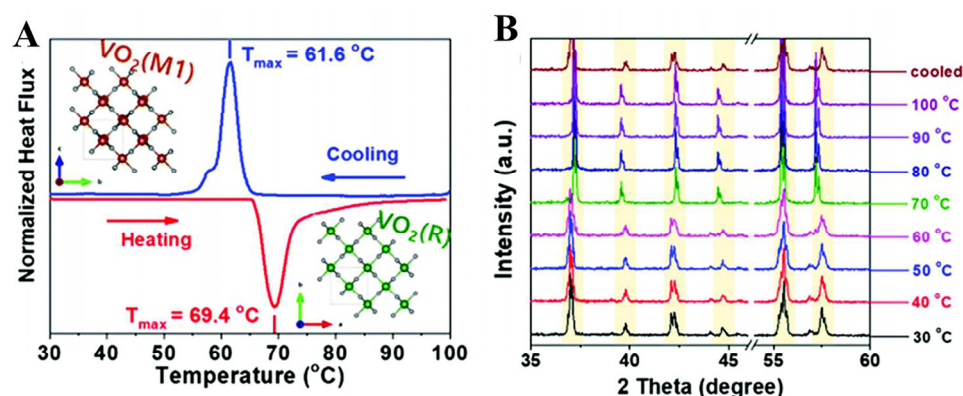


**Figure 4.** (A) DSC analysis and (B) in situ heating XRD patterns of as-synthesized  $\text{VO}_2$  ( $M_1$ ) nanobelts in the temperature range of 30–100 °C. Reproduced with permission [42]. Copyright 2022 Royal Society of Chemistry.

**Table 1.** Representative V-based oxide and hydroxide electrocatalysts for HER and OER.

Catalysts	Overpotential for HER (mV@ 10 mA cm <sup>-2</sup> )	Overpotential for OER (mV@ 10 mA cm <sup>-2</sup> )	Stability	Electrolyte	Substrate	Preparation Method	Ref.
NiCo/ $\text{V}_2\text{O}_3$ /C	23	—	50 h @ 10 mA cm <sup>-2</sup>	1 M KOH	NF	Gas–solid reaction	[39]
$\text{VO}_2$ -NiS <sub>2</sub>	96	220	10 h @ 10 mA cm <sup>-2</sup>	1 M KOH	CC	Hydrothermal	[1]
$\text{Co}(\text{OH})_2$ / $\text{V}_2\text{O}_5$	—	320	15 h @ 10 mA cm <sup>-2</sup>	1 M KOH	GCE	Hydrothermal	[46]

Table 1. Cont.

Catalysts	Overpotential for HER (mV@ 10 mA cm <sup>-2</sup> )	Overpotential for OER (mV@ 10 mA cm <sup>-2</sup> )	Stability	Electrolyte	Substrate	Preparation Method	Ref.
IrCo@V <sub>2</sub> O <sub>5</sub>	92	280	24 h @ 10 mA cm <sup>-2</sup>	1 M KOH	GCE	Microwave hydrothermal	[47]
in-NiV-LDH	114	—	100 h @ 10 mA cm <sup>-2</sup>	1 M KOH	NF	Hydrothermal	[48]
Ru-CoV-LDH	32	230	45 h @ 20 mA cm <sup>-2</sup>	1 M KOH	NF	Hydrothermal	[49]
Se-NiV-LDH	85	198	10 h @ 50 mA cm <sup>-2</sup>	1 M KOH	NF	Hydrothermal	[50]
A-NiFeV-LDH	—	250	100 h @ 10 mA cm <sup>-2</sup>	1 M KOH	NF	Hydrothermal	[51]
NiCo-LDH @NiCoV-LDH	80	260	40 h @ 10 mA cm <sup>-2</sup>	1 M KOH	NF	Hydrothermal electrodeposition	[52]
CoFe-NiV	—	150	12 h @ 10 mA cm <sup>-2</sup>	1 M PBS	SS	Hydrothermal	[53]
NiV-LDH-CoP	93	—	200 h @ 1 A cm <sup>-2</sup>	0.5 M H <sub>2</sub> SO <sub>4</sub>	CC	Hydrothermal annealing electrodeposition	[54]
Ni <sub>3</sub> S <sub>2</sub> @NiV	126	190	100 h @ 10 mA cm <sup>-2</sup>	1 M KOH	NF	Hydrothermal	[55]

Note: NF = Ni foam, CC = carbon cloth, glassy carbon electrode = GCE, stainless steel = SS.

### 3.1.2. OER Performance

Najafi et al. obtained the metallic rutile phase VO<sub>2</sub> by topochemically transforming liquid-phase exfoliated VSe<sub>2</sub> in an Ar-H<sub>2</sub> atmosphere. The obtained 2D VO<sub>2</sub> (R) nanosheets had a porous morphology, increasing the specific surface area of the material while introducing defect sites. When tested in 1 M KOH solution, the 2D VO<sub>2</sub> (R) only acquired the overpotential of 209 mV to obtain the current density of 10 mA cm<sup>-2</sup> [56]. Crystalline–amorphous composite engineering is a highly efficient approach to improving the OER performance of electrocatalysts. Zhou et al. designed amorphous–crystalline VO<sub>2</sub>/NiS<sub>2</sub> heterostructures with good OER performance. The authors found that amorphous VO<sub>2</sub> was easily dissolved in the KOH electrolyte during the OER, which induced abundant oxygen vacancies in the NiOOH active phase generated in situ by NiS<sub>2</sub>, thus greatly improving the OER activity. A current density of 10 mA cm<sup>-2</sup> can be acquired with an overpotential of only 272 mV [1]. Tang et al. prepared V<sub>2</sub>O<sub>5</sub>/Co(OH)<sub>2</sub> composites at room temperature. The V<sup>5+</sup> of V<sub>2</sub>O<sub>5</sub> can oxidize the Co<sup>2+</sup> of Co(OH)<sub>2</sub> to Co<sup>3+</sup>, inducing the easier generation of CoOOH species favorable for the OER [46]. The OER performance of representative V-based oxides are listed in Table 1.

In summary, the high valence species of vanadium-based oxides will have a synergistic effect with the transition metal-based hydroxides and sulfides that are composited with them, which is favorable for allowing the electrocatalysts to more easily generate the true high-valence OER active species.

### 3.2. Vanadium-Based Hydroxides

Pure V monometallic hydroxides in water splitting have rarely been studied, and the V-based hydroxide electrocatalysts reported for the HER and OER are mainly V ions and other transition metal ions (Fe, Co, Ni, etc.) forming bimetallic layered hydroxides (LDHs) as well as derived trimetallic layered hydroxides (LTHs) [57–60].

LDHs are simple to synthesize and have a multilayered, relatively open structure with the following chemical formula: [M<sup>II</sup><sub>1-x</sub>M<sup>III</sup><sub>x</sub>(OH)<sub>2</sub>]<sub>x</sub><sup>+</sup>A<sup>n-</sup><sub>x/n</sub>·yH<sub>2</sub>O (M is the metal cation and A<sup>n-</sup> is the anion,) allowing for the rapid diffusion of reactants and products, accelerating the mass transfer process of the reaction [61,62]. Therefore, more and more studies have been conducted on V-based hydroxide electrocatalysts in the field of water electrolysis, especially in the OER [29]. The role played by the element V in LDHs and LTHs has also been explored more by researchers at the same time [63]. In this paper, the

performance, modification strategies, and the role of V elements in the above-mentioned V-based hydroxides for the HER and OER are summarized.

### 3.2.1. HER Performance

The main V-based hydroxides that have been reported for the HER are layered bimetallic hydroxides, such as NiV and CoV, and derived ternary layered hydroxides [49,64]. Generally, the element V should theoretically be in the trivalent state; however, due to oxidation during synthesis, trivalent vanadium is easily oxidized to higher valence states of tetravalent and pentavalent vanadium in NiV LDHs. Therefore, the influence of the valence state of V in the NiV system on its HER performance is worth exploring. Based on this, Feng's team synthesized in-NiV-LDHs (the Ni source was nickel foam) and ex-NiV-LDHs (the Ni source was  $\text{NiCl}_2 \cdot 6\text{H}_2\text{O}$ ) by adjusting the type of nickel source in a one-step hydrothermal synthesis process. The main difference is that the valence state of V in in-NiV-LDHs is significantly lower than that in ex-NiV-LDHs. The authors analyzed Ni-V-O as a model (Figure 5A) and concluded that the low valence states of vanadium ( $\text{V}^{3+}$  and  $\text{V}^{4+}$ ) accelerated the electron aggregation, which was favorable for the dissociation of water molecules. On the other hand, the low valence states of vanadium ( $\text{V}^{3+}$  and  $\text{V}^{4+}$ ) regulated the adsorption/desorption capacity of  $\text{H}_{\text{ads}}$ , thus enhancing the HER performance [48].

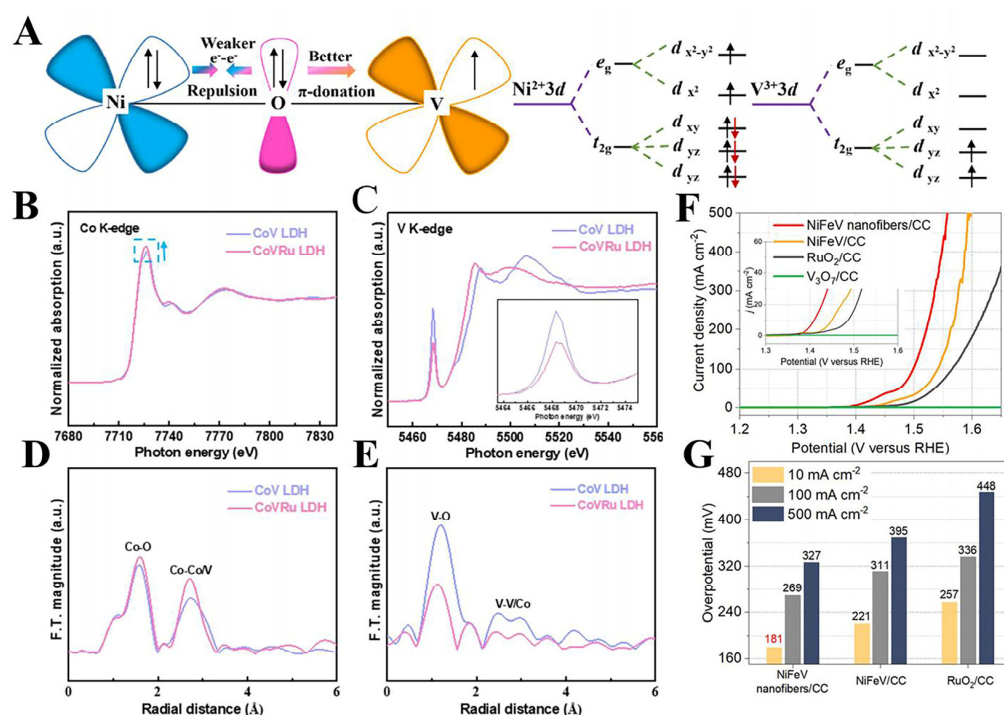


**Figure 5.** (A) Schematic representations of the electronic coupling between Ni and V. Reproduced with permission [48]. Copyright 2022 Elsevier. (B,C) Normalized XANES spectra of Co K-edge and V K-edge. (D,E) Fourier-transformed EXAFS spectra for CoV LDH and CoVRu LDH. Reproduced with permission [65]. Copyright 2023 Elsevier. (F) LSV curves and (G) the overpotentials at 10, 100, and 500  $\text{mA cm}^{-2}$  for NiFeV nanofibers.

In addition, it has been shown that a change in V coordination structure has a large impact on its HER performance in V-based LDHs; Zeng et al. synthesized CoV-LDHs and CoVRu LDHs with hexagonally shaped nanosheets by a hydrothermal method, and the test results showed that the HER performance was greatly enhanced after Ru was anchored in the CoV LDHs. As shown in Figure 5B,E, XANES and EXAFS from the CoV LDHs and CoVRu LDHs indicate that there is no significant change in the coordination environment of Co after the addition of Ru. However, there is a considerable change in the coordination environment of V. This suggests that the introduction of atomically



dispersed Ru with high electronegativity leads to the structural distortion and space charge redistribution of V octahedra, which optimizes the HER kinetics [65]. Similarly, Li et al. also observed from XPS that the doping of Ru has a significant effect on the electronic structure of CoV-LDHs. The Tafel slope indicates that for the HER, when Ru is doped effectively it reduces the energy barrier of the Volmer step, which in turn improves the electrocatalytic hydrogen precipitation performance [49]. The HER performance of representative V-based hydroxides are listed in Table 1. In conclusion, the valence state and coordination of V have a great influence on the HER performance of V-based hydroxides.

### 3.2.2. OER Performance

Angnes et al. systematically summarized the progress of NiV LDHs as electrocatalysts for the HER and OER, and multiple studies have demonstrated that NiV-LDHs have optimal OER performance when Ni:V = 3:1 [29]. Although many works show that V-doped Ni-based and NiFe-based materials have good OER effects, there is a lack of in-depth discussion and characterization on whether the V ions are actually doped into the lattice in the subject materials to replace the position of Ni ions, and how to improve the OER catalytic activity of the subject materials.

Jiang et al. developed a series of Fe/V-doped  $\alpha$ -Ni(OH)<sub>2</sub> ultrathin nanosheet arrays (Ni<sub>3</sub>Fe<sub>1-x</sub>V<sub>x</sub>/CFP), it can be concluded that both Fe and V ions occupy the position of Ni in Ni(OH)<sub>2</sub> using Wavelet variation curves (WT) from EXAFS. In addition, in situ XAFS tests indicate that V in Ni<sub>3</sub>Fe<sub>0.5</sub>V<sub>0.5</sub> has a highly distorted coordination structure with a short V-O bond length, and further contraction during the OER. Meanwhile, DFT + U theoretical calculations show that the V site at the aggregation of Fe and V atoms has the optimal OER oxygen intermediate state binding energy and the lowest theoretical overpotential. Additionally, the synergistic electronic interactions between Ni, Fe, and V are well explained by metal ion valence electron structure analysis. As some electrons are transferred from Ni and Fe to V via the oxygen bridge, the electron density of the V center increases, and thus, the high-valence V intermediate is stabilized under OER conditions. More importantly, according to Sabatier's principle, the strong bond between the high-valence-state V and adsorbed oxygen in the reaction intermediates can be weakened to a certain extent. This facilitates the release of oxygen formed by the oxidation of water from the V site [57].

Zhang et al. developed a novel interfacial atom substitution strategy to prepare V atom-doped NiFeV nanofibers for efficient alkaline OER electrocatalysis. It was found that the interfacial atom substitution growth of V can maximize the effect of V atoms on the valence states of Fe and Ni atoms and increase the proportion of high-valence Fe atoms compared to the traditional one-pot method of adding V atoms. This greatly enhances the OER kinetics of the NiFeV and ultimately improves the OER performance. As shown in Figure 5F,G, the overpotential of the NiFeV material is only 181 mV (10 mA cm<sup>-2</sup>), and it can be stably operated for more than 20 h at 100 mA cm<sup>-2</sup> [66]. As demonstrated by the examples above, the vanadium in vanadium-based hydroxides plays a dual role: it acts as an active site and enhances the OER performance by modulating the electronic structures of the neighboring metal ions. The OER performance of representative V-based hydroxides are listed in Table 1.

However, it is worth noting that V ions are not necessarily active sites in hydroxides such as LDHS, LTHS, etc. Nejadi et al. synthesized ZnFe-VO<sub>4</sub>-LDH by co-precipitation, although ZnFe-VO<sub>4</sub>-LDH had better OER properties than ZnFe-NO<sub>3</sub>-LDH and ZnFe-MoO<sub>4</sub>-LDH. The authors concluded that the vanadate ions only act as spacers, favoring the mass-transfer process, while the real electrocatalytic sites are the Zn<sup>2+</sup> and Fe<sup>3+</sup> sites [67].

### 3.3. Vanadate

Transition metal vanadates (MV<sub>x</sub>O<sub>y</sub>) can be regarded as a combination of transition metal ions and vanadium oxides. Currently, CoV<sub>x</sub>O<sub>y</sub>, NiV<sub>x</sub>O<sub>y</sub>, and other material systems have received wide attention for their good electrocatalytic catalytic performance [68,69]. Their excellent performance can be attributed to the following three aspects: Firstly, the

doping of transition metal ions such as Ni and Co makes the vanadates have better electrical conductivity than vanadium oxides and vanadium hydroxides. Secondly, in the elemental composition of vanadate, V is a pre-transition metal element, while the doped transition metal elements are mostly Fe, Co, Ni, and other late-transition metal elements. Since there is a prominent difference between the adsorption of pre-transition metal elements and late-transition metal elements on the reaction intermediates [65,70], the rational design of vanadate materials can optimize the adsorption of the reaction intermediates, and then promote the reaction kinetics. Finally, the electronic structure of  $MV_xO_y$  can be optimized by taking advantage of the multiple oxidation valence states of V and the adjustable stoichiometric ratio of  $MV_xO_y$  to improve the performance of electrocatalytic hydrogen production. The following is a summary of the HER and OER performances of  $MV_xO_y$  and their modification strategies in recent years.

### 3.3.1. HER Performance

Constructing a heterostructure of vanadate and transition metal can optimize the electronic structure of the material and thus optimize the HER kinetics. Pan et al. synthesized Ni-Co<sub>2</sub>VO<sub>4</sub> on NF by hydrothermal and solid-phase sintering and only required 50, 267, and 329 mV to reach current densities of 10, 500, and 1000 mA cm<sup>-2</sup>, respectively. The authors concluded that the excellent HER performance of Ni-Co<sub>2</sub>VO<sub>4</sub> can be ascribed to two aspects: Firstly, the mesoporous nanosheets with a large specific surface area possess a large electrochemically active area, which also contributes to the desorption of surface bubbles and promotes the mass transfer kinetics. On the other hand, the heterostructure formed by Ni and Co<sub>2</sub>VO<sub>4</sub> can facilitate the adsorption of water molecules and the intrinsic activity of HER by modulating the interfacial electronic structure to form electron-poor/rich species [71]. Zhou et al. anchored hollow CoV<sub>2</sub>O<sub>6</sub> nanocubes to Mxene (V<sub>2</sub>CT<sub>x</sub>). The V<sub>2</sub>CT<sub>x</sub> lattice tensile strain could promote the ion transfer of transition metals due to the increased layer spacing. Meanwhile, the heterostructure between CoV<sub>2</sub>O<sub>6</sub> and V<sub>2</sub>CT<sub>x</sub> Mxene could optimize the adsorption energies of H- and O-containing intermediates to obtain the optimal  $\Delta G_{H^*}$  for the HER [72]. The HER performance of representative vanadate are listed in Table 2.

**Table 2.** Representative vanadate electrocatalysts for HER and OER.

Catalysts	Overpotential for HER (mV@ 10 mA cm <sup>-2</sup> )	Overpotential for OER (mV@ 10 mA cm <sup>-2</sup> )	Stability	Electrolyte	Substrate	Preparation Method	Ref.
Ni-Co <sub>2</sub> VO <sub>4</sub>	50	—	140 h @ 50 mA cm <sup>-2</sup>	1 M KOH	NF	Gas–solid reaction	[71]
TS-V <sub>2</sub> CT <sub>x</sub> /CoV <sub>2</sub> O <sub>6</sub>	32.2	235	24 h @ 10 mA cm <sup>-2</sup>	1 M KOH	NF	Chemical etching annealing	[72]
Co <sub>3</sub> V@C/Co <sub>2</sub> VO <sub>4</sub>	51	—	100 h @ 100 mA cm <sup>-2</sup>	1 M KOH	NF	Gas–solid reaction	[73]
N-Co <sub>2</sub> V <sub>2</sub> O <sub>7</sub>	87	244	170 h @ 100 mA cm <sup>-2</sup>	1 M KOH	NF	Gas–solid reaction	[74]
S-Co <sub>3</sub> V <sub>2</sub> O <sub>8</sub>	—	227	12 h @ 50 mA cm <sup>-2</sup>	1 M KOH	NF	Hydrothermal	[75]
Fe-Co <sub>2</sub> VO <sub>4</sub>	—	205	100 h @ 20 mA cm <sup>-2</sup>	1 M KOH	NF	Gas–solid reaction	[76]
S-NiCoVO <sub>x</sub>	—	248	30 h @ 50 mA cm <sup>-2</sup>	1 M KOH	NF	Hydrothermal	[77]
Co <sub>1.5</sub> Fe <sub>1.5</sub> V <sub>2</sub> O <sub>8</sub>	—	290	10 h @ 10 mA cm <sup>-2</sup>	1 M KOH	CFP	Hydrothermal	[78]

Note: CFP = Carbon fiber paper.

### 3.3.2. OER Performance

Non-metallic element doping is an important approach to enhance the OER performance of cobalt vanadate systems. Luo et al. synthesized nitrogen-doped Co<sub>2</sub>V<sub>2</sub>O<sub>7</sub> on NF by hydrothermal and low-temperature ammoniation. As shown in Figure 6A, DFT

calculations show that N doping can fine-tune the d-band center and band gap to promote intermediate adsorption and electron movement (Figure 6B,C). As depicted in Figure 6D,E, the N-Co<sub>2</sub>V<sub>2</sub>O<sub>7</sub>/NF only required an overpotential of 310 mV to reach a current density of 100 mA cm<sup>-2</sup> with a Tafel slope of only 56.3 mV dec<sup>-1</sup> [74]. Gyanprakash D et al. synthesized S-Co<sub>3</sub>V<sub>2</sub>O<sub>8</sub> by hydrothermal synthesis, which had higher electrical conductivity than Co<sub>3</sub>V<sub>2</sub>O<sub>8</sub>, reaching a current density of 100 mA cm<sup>-2</sup> with an overpotential of only 227 mV for S-Co<sub>3</sub>V<sub>2</sub>O<sub>8</sub> [75].

It is well known that V ions are soluble in aqueous electrolytes, which can easily lead to the surface reconstruction of catalysts. Therefore, the form of V ions in cobalt vanadate in alkaline environments and their effect on the activity and stability of the electrocatalyst need to be explored. Li et al. prepared Fe-modified Co<sub>2</sub>VO<sub>4</sub> by hydrothermal and hydrogen reduction to induce controlled surface reconstruction by activating lattice oxygen and cation leaching. Through a combination of theoretical and experimental results, the authors found that Fe substitution plays a crucial role in accelerating Co peroxidation and introduces a great deal of structural flexibility due to elevated O 2p levels and optimized Co-O covalency. Meanwhile, V ions are present in the base-resistant form of V<sub>2</sub>O<sub>3</sub> during CV cycling and are incorporated into the surface-constructed CoOOH layer to efficiently prevent the excessive loss of reactive species and lattice oxygen. Thanks to the modification of Fe and the stabilizing effect of V ions, Co<sub>2</sub>Fe<sub>0.25</sub>V<sub>0.75</sub>O<sub>4</sub> requires only an overpotential of 205 mV to acquire a current density of 10 mA cm<sup>-2</sup> for the OER [76].

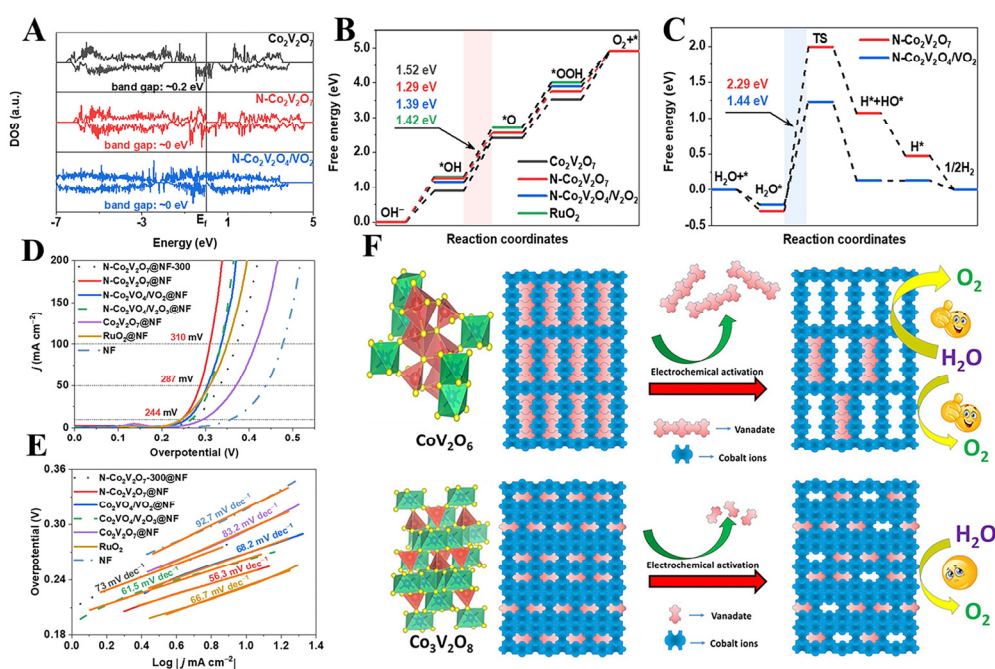


**Figure 6.** (A) The DOS of Co<sub>2</sub>V<sub>2</sub>O<sub>7</sub>, N-Co<sub>2</sub>V<sub>2</sub>O<sub>7</sub>, and N-Co<sub>2</sub>V<sub>2</sub>O<sub>4</sub>/VO<sub>2</sub>. (B) Gibbs free energy diagrams of Co<sub>2</sub>V<sub>2</sub>O<sub>7</sub>, N-Co<sub>2</sub>V<sub>2</sub>O<sub>7</sub>, and N-Co<sub>2</sub>V<sub>2</sub>O<sub>4</sub>/VO<sub>2</sub> for the OER. (C) Gibbs free energy diagrams of N-Co<sub>2</sub>V<sub>2</sub>O<sub>7</sub> and N-Co<sub>2</sub>V<sub>2</sub>O<sub>4</sub>/VO<sub>2</sub> for the HER. (D) The OER polarization curves. (E) Tafel plot. Reproduced with permission [74]. Copyright 2023 Elsevier. (F) Schematic diagram of the structure and electrochemical activation of Co<sub>3</sub>V<sub>2</sub>O<sub>8</sub> and CoV<sub>2</sub>O<sub>6</sub>. Reproduced with permission [79]. Copyright 2021 American Chemical Society.

Mondal et al. found that the state of polymerization of vanadate has a significant effect on its OER performance. The authors first synthesized Co<sub>3</sub>V<sub>2</sub>O<sub>8</sub> and CoV<sub>2</sub>O<sub>6</sub> by the sol-gel method. The difference between Co<sub>3</sub>V<sub>2</sub>O<sub>8</sub> and CoV<sub>2</sub>O<sub>6</sub> is that the element V in Co<sub>3</sub>V<sub>2</sub>O<sub>8</sub> is in a discrete [VO<sub>4</sub>]<sup>3-</sup> form, while in CoV<sub>2</sub>O<sub>6</sub> it exists as polymerized VO<sub>3</sub> units ([VO<sub>3</sub>]<sub>n</sub>)<sup>n-</sup>. The authors suggest that the activity of cobalt vanadate arises from the etching of vanadate in the precatalyst by electrochemical activation (Figure 6F). The

resulting higher surface reconstruction exposes more catalytically active cobalt sites. As shown in the figure, compared to the discrete  $[\text{VO}_4]^{3-}$  in  $\text{Co}_3\text{V}_2\text{O}_8$ , the polymer structure of the vanadate bias  $([\text{VO}_3]_n)^{n-}$  in  $\text{CoV}_2\text{O}_6$  promotes the etching phenomenon, thereby exposing a larger electrochemically active area [79]. The construction of multicomponent oxide heterostructures is an effective strategy to improve the performance of the OER. Li et al. obtained  $\text{NiCoVO}_x$  ( $\text{Ni}(\text{VO}_3)_2/\text{Co}_2\text{V}_2\text{O}_7$ ) by a hydrothermal method. The  $\text{NiCoVO}_x$  requires only an overpotential of 217 mV to reach a current density of  $50 \text{ mA cm}^{-2}$ , thanks to the synthesized flower-like arrays and synergistic effect of  $\text{Ni}(\text{VO}_3)_2$  and  $\text{Co}_2\text{V}_2\text{O}_7$  [80]. In conclusion, vanadates, as a highly promising OER electrocatalyst, require further investigation into their mechanisms during the OER process. The OER performance of representative vanadate are listed in Table 2.

### 3.4. Vanadium-Based Dichalcogenides

#### 3.4.1. Vanadium-Based Sulfides

Transition metal disulfides have a graphene-like two-dimensional layered structure with the general structural formula  $\text{MS}_2$ , where M stands for the transition metal (M = Mo, W, V, Nb, etc.)  $\text{MS}_2$  is constructed in the S-M-S pattern, where the metal atoms provide four electrons to bond with two sulfur atoms to achieve a bonded state within the molecular layer of the transition metal sulfide. In addition, the sulfur atoms have a lone pair of electrons on their surface which do not have any unpaired bonds. This prevents them from reacting to other environments [81–83]. Compared to  $\text{MoS}_2$ , the typical TMDs, 1T- $\text{VS}_2$  and 2H- $\text{VS}_2$ , have metallic properties and good conductivity. Moreover, their graphene-like structures provide a larger specific surface area [84,85]. In recent years, the above characteristics of  $\text{VS}_2$  have led to a rapid increase in its study for water splitting, especially in the HER [86,87]. The following summarizes the recent HER and OER performance of  $\text{VS}_2$ , as well as the modification strategies used.

#### HER Performance

A series of computational and experimental results illustrate that  $\text{VS}_2$  has metallic properties and great potential for the HER. For example, Zhang et al. used DFT to calculate the adsorption capacity of  $\text{VS}_2$  for hydrogen atoms and found that the  $\Delta G_{\text{H}^*}$  of the pristine  $\text{VS}_2$  bases in the 2H and 1T phases were 0.26 eV and  $-0.16$  eV, respectively. These results are close to the bases of Pt. ( $\Delta G_{\text{H}^*} = -0.09$  eV), suggesting that  $\text{VS}_2$  has similar HER activity to Pt [88]. Currently,  $\text{VS}_2$ , along with  $\text{MoS}_2$  and other TMDs, mostly exhibits its active sites at the edge, whereas the unreactive basal plane restricts the further improvement of  $\text{VS}_2$  HER activity. Consequently, significant efforts have been dedicated to enhancing the  $\text{VS}_2$  basal plane activity in order to improve the HER performance of  $\text{VS}_2$  [88,89]. Zhang et al. synthesized  $\text{VS}_2$  with a larger layer spacing ( $\sim 1$  nm) by a simple hydrothermal method, which was expanded by  $\sim 74\%$  compared with the layer spacing of pristine  $\text{VS}_2$  (0.575 nm). Due to the expanded layer spacing,  $\text{VS}_2$  introduces more in-plane defects. Meanwhile, theoretical calculations and experimental results show that modulation of the intrinsic defects excites the catalytic activity of the  $\text{VS}_2$  basal plane and improves the stability. For the HER, an overpotential of only 43 mV is required to obtain the current density of  $10 \text{ mA cm}^{-2}$ . After a 60 h stability test, no significant current decay was found, indicating the excellent long-term stability of  $\text{VS}_2$  with expanded layer spacing [90]. Transition metal ion doping is also an important strategy to enhance the basal plane activity of  $\text{VS}_2$  [91,92]. He et al. prepared Mo-doped  $\text{VS}_2$  using a one-step hydrothermal method. The results showed that the Mo- $\text{VS}_2$  HER performance was greatly improved with respect to  $\text{VS}_2$ . The theoretical calculations mean that the enhanced performance of the catalyst is due to the fact that the Mo dopant reduces the free energy of hydrogen adsorption on the S-site (Figure 7A–C), which results in the enhancement of the catalytic activity for the basal plane [93].

In addition to activating the basal activity of  $\text{VS}_2$  through doping and modulating intrinsic defects, fully exposing the  $\text{VS}_2$  edge active sites through composite strategies as

well as morphology modulation strategies is also an effective way to enhance the HER performance of VS<sub>2</sub>-based electrocatalysts. For example, Pandurangan's group successfully synthesized VS<sub>2</sub>/rGO by one-step hydrothermal synthesis of VS<sub>4</sub>/rGO, and then the target material VS<sub>2</sub>/rGO was synthesized by calcination. The presence of rGO resulted in more dispersed VS<sub>2</sub> nanosheets, thus exposing more edge structures [94]. Patil et al. used a solvent-thermal method to prepare micrometer floral VS<sub>2</sub>. The HER performance of VS<sub>2</sub> was enhanced by varying the ratio of ethylene glycol and water in the solvent to modulate the catalyst morphology, which in turn exposed more edge active sites [95]. The HER performance of representative Vanadium-based sulfides are listed in Table 3. In conclusion, VS<sub>2</sub> emerges as a promising electrocatalyst for HER. Nevertheless, how to effectively activate its basal plane is still worth researching.

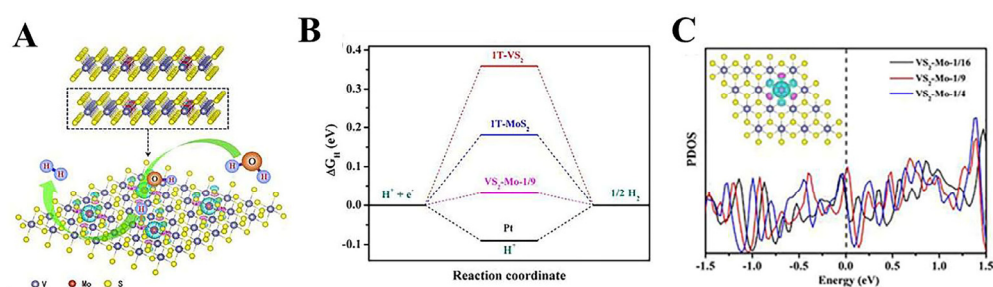


**Figure 7.** (A) Schematic illustration of the catalytic HER sites for the Mo-doped VS<sub>2</sub>. (B)  $\Delta G_{H^*}$  of S sites on the basal plane for 1T-VS<sub>2</sub>, 1T-MoS<sub>2</sub>, and VS<sub>2</sub>-Mo-1/9. (C) Projected p-orbital density of states of S for the Mo-doped VS<sub>2</sub>. Reproduced with permission [93]. Copyright 2020 Elsevier.

**Table 3.** Representative V-based dichalcogenides electrocatalysts for HER and OER.

Catalysts	Overpotential for HER (mV@ 10 mA cm <sup>-2</sup> )	Overpotential for OER (mV@ 10 mA cm <sup>-2</sup> )	Stability	Electrolyte	Substrate	Preparation Method	Ref.
Mo/Co-VS <sub>2</sub>	63	248	36 h @ 10 mA cm <sup>-2</sup>	1 M KOH	CC	Hydrothermal	[92]
Mo-VS <sub>2</sub>	243	—	25 h @ 10 mA cm <sup>-2</sup>	1 M KOH	GCE	Hydrothermal	[93]
MoS <sub>2</sub> /VS <sub>2</sub>	291	—	16 h @ 15 mA cm <sup>-2</sup>	0.5 M H <sub>2</sub> SO <sub>4</sub>	GCE	Hydrothermal	[96]
Ru-VS <sub>2</sub>	—	245 (50 mA cm <sup>-2</sup> )	20 h @ 10 mA cm <sup>-2</sup>	0.1 M KOH	CC	Hydrothermal	[97]
Ni <sub>3</sub> S <sub>2</sub> /VS <sub>2</sub>	—	227	20 h @ 10 mA cm <sup>-2</sup>	1 M KOH	NF	Hydrothermal	[98]
ReSe <sub>2</sub> -VSe <sub>2</sub>	71	—	120 h @ 20 mA cm <sup>-2</sup>	0.5 M H <sub>2</sub> SO <sub>4</sub>	GCE	Annealing	[99]
P,Fe-(VCo)Se <sub>2</sub>	51	250 (50 mA cm <sup>-2</sup> )	50 h @ 50 mA cm <sup>-2</sup>	1 M KOH	NF	Hydrothermal	[100]
VSe <sub>2</sub> /rGO	110	280	2.7 h @ 5 mA cm <sup>-2</sup>	1 M KOH	NF	Hydrothermal	[101]

### OER Performance

There are fewer studies about the OER performance of VS<sub>2</sub>. Some calculations have shown that monolayer VS<sub>2</sub> is a good catalyst candidate for OER [102]. Qin et al. systematically explored the OER activity of a series of single transition metal atoms (Fe, Co, Ni, Ti, Mn, Hf, Zr, etc.) through first-principles calculations. The results showed that Ni@VS<sub>2</sub> has the lowest OER overpotential (0.31 V) and its favorable OER performance can be attributed to the superior  $\Delta G(O^*)$  [103].

Hou et al. synthesized Ru-VS<sub>2</sub> on carbon cloth by the one-step hydrothermal method. The in situ Raman spectroscopy showed that the Ru atomic clusters would be electro-oxidized to RuO<sub>2</sub> during the OER process, offering a large number of active sites. The VS<sub>2</sub> substrate mainly plays the role of protecting the Ru nucleus. Theoretical calculations

show that electrons crossing the Ru/VS<sub>2</sub> interface converge toward the electro-oxidized Ru clusters, while the electronic coupling of the Ru 3p and O 2p orbitals promotes the positive shift of the Ru Fermi energy level and optimizes the adsorption capacity of Ru for intermediates. As a result, the Ru-VS<sub>2</sub>@CC required only an overpotential of 245 mV to obtain the current density of 50 mA cm<sup>-2</sup> [97].

Dhakal et al. synthesized 3D CoMnS<sub>2</sub>@1T-Fe-VS<sub>2</sub> by a two-step hydrothermal method, which acquired only an overpotential of 260 mV to reach the current density of 20 mA cm<sup>-2</sup>. Its excellent OER performance can be ascribed to the synergistic catalysis of the activated basal and edge sites of the CoMnS<sub>2</sub> nucleus and the 1T-Fe-VS<sub>2</sub> shell. The OER performance of representative Vanadium-based sulfides are listed in Table 3. Overall, the current OER research about VS<sub>2</sub> mainly focuses on using it as a substrate, loading and protecting active sites such as single atoms and clusters, or compounding it with other materials to improve the OER performance. The performance of VS<sub>2</sub> as an OER electrocatalyst by itself is not too satisfactory [104].

### 3.4.2. Vanadium-Based Selenides

VSe<sub>2</sub> is also a member of TMDs, and Se belongs to the same main group (VIA) as S. The chemical properties are similar between S and Se, but at the same time, there are many differences. Se is more metallic than S, which exhibits better electrical conductivity. At the same time, the ionization energy of Se is smaller than that of S. Therefore, VSe<sub>2</sub> and VS<sub>2</sub> have a similar ionization energy. Therefore, the physicochemical properties and electrocatalytic performances of VSe<sub>2</sub> and VS<sub>2</sub> are different [105,106]. The following is a summary of the HER and OER performances of VSe<sub>2</sub>, as well as the modification strategies in recent years.

#### HER Performance

Contrary to the metallic nature of the 1T-VS<sub>2</sub> and 2H-VS<sub>2</sub>, the 2H-VSe<sub>2</sub> phase predominantly displays semiconducting characteristics [107]. Hence, the conversion of 2H-VSe<sub>2</sub> to the metallic 1T phase of VSe<sub>2</sub> through crystalline phase engineering can enhance the conductivity of the material and accelerate the electron transfer for HER. Zhao et al. prepared metallic VSe<sub>2</sub> nanosheets with a thickness of about 0.4 nm by a one-pot colloidal route and tested the powder on a rotating disk electrode, which required an overpotential of only 206 mV to reach the density of 10 mA cm<sup>-2</sup> [108]. Kwak et al. prepared the ReSe<sub>2</sub>-VSe<sub>2</sub> (Re<sub>1-x</sub>V<sub>x</sub>Se<sub>2</sub>) alloy nanosheets by colloidal reaction. The authors found that increasing x makes the nanosheets more metallic and transforms VSe<sub>2</sub> to 1T phase at x = 0.5–0.6. It requires only an overpotential of 77 mV under acidic conditions to reach the current density of 10 mA cm<sup>-2</sup> [99].

VSe<sub>2</sub> has a layered structure with active sites mainly found at the edges like VS<sub>2</sub>. Therefore, the activation of the inert basal plane inside VSe<sub>2</sub> through defect engineering and the increase in the density of active sites at the edges of VSe<sub>2</sub> through morphology modification strategies are important ways to enhance the HER performance of VSe<sub>2</sub> [109–111]. Zhang et al. reported a VSe<sub>2</sub> nanosheet with single-atom (SA) V defects and Se vacancy defects. The experimental and computational results showed that the presence of double defects effectively activated the inert substrate of VSe<sub>2</sub>, and the HER performance was enhanced. Its overpotentials to reach the current densities of 10 mA cm<sup>-2</sup> under acidic, alkaline, and neutral conditions were 67.2, 72.3, and 122.3 mV, respectively [112]. Wang et al. obtained VSe<sub>2</sub> quantum dots (3–6 nm) with a high density of edge sites by the tip sonication of VSe<sub>2</sub> nanosheets. Compared with VSe<sub>2</sub> nanosheets, VSe<sub>2</sub> quantum dots have a high density of edge-active sites, which significantly improves their HER performance [113]. The HER performance of representative Vanadium-based selenides are listed in Table 3.

#### OER Performance

Recent work has shown that VSe<sub>2</sub> has room-temperature ferromagnetism [114]. For ferromagnetic catalysts, an external magnetic field can optimize the kinetics of OER by

modulating the electronic state of the material [115,116]. Inspired by this, Chen et al. confined monodisperse 1T-VSe<sub>2</sub> nanoparticles on an amorphous carbon substrate by simple pulsed laser deposition (PLD) with rapid thermal annealing (RTA) (Figure 8A). Stimulated by an external magnetic field of 800 mT, the confined 1T-VSe<sub>2</sub> nanoparticles exhibited highly efficient OER performance with an overpotential of 228 mV for the densities of 10 mA cm<sup>-2</sup>, which is superior to that of 1T-VSe<sub>2</sub> without an applied magnetic field. Theoretical calculations showed that the magnetic field could promote the surface charge transfer kinetics of 1T-VSe<sub>2</sub> and change the free energy of adsorption of \*OH (Figure 8B,C), thereby ultimately increasing the intrinsic activity of the catalyst [117]. The OER performance of representative Vanadium-based selenides are listed in Table 3. Consequently, the intrinsic OER activity of electrocatalysts such as VS<sub>2</sub> and VSe<sub>2</sub>, which is not ideal, can be enhanced by optimizing their adsorption towards oxygen-containing intermediates through the application of external fields during testing.

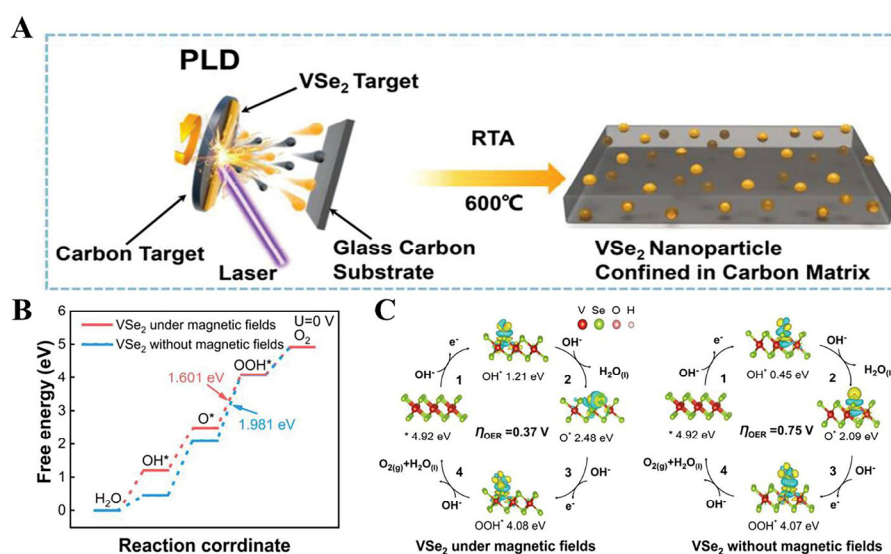


**Figure 8.** (A) The schematic illustration for the synthesis process of confined 1T-VSe<sub>2</sub> nanoparticles. (B) Gibbs free-energy diagram and (C) calculated charge density difference plot of OER steps of 1T-VSe<sub>2</sub> under magnetic fields and without magnetic fields. Reproduced with permission [117]. Copyright 2023, Wiley-VCH.

### 3.5. Vanadium-Based Nitrides

Transition metal nitrides (TMNs), with their Pt-like electronic structure and catalytic behavior, are strong contenders for replacing noble metal catalysts for water splitting [18,118,119]. VN has a face-centered cubic crystal structure. The bonding between vanadium (V) and nitrogen (N) atoms results in a reduction in the d-band of the metallic vanadium, leading to an increase in the density of states at the Fermi energy level. As a result, VN exhibits electrical conductivity and resistance to corrosion. The aforementioned characteristics of VN make it a strong contender to replace precious metal catalysts [120–122]. However, the HER performance of VN is limited by its excessively strong hydrogen adsorption-free energy [123,124]. Meanwhile, the development of VN-based bifunctional electrocatalysts for water splitting remains challenging. The performance of VN in the HER, as well as in the OER and its modification strategies, are presented below.

#### 3.5.1. HER Performance

The excessively strong hydrogen adsorption-free energy of VN limits the further enhancement of its HER performance. Thus, regulating the hydrogen adsorption-free energy of VN by modulating the electronic structure of VN is an effective strategy to improve the VN-based HER performance. Feng et al. employed Co, V-MIL-88B as a precursor, and subjected it to high-temperature ammoniation, resulting in the formation

of shuttle-like ends composed of Co/VN (Figure 9A,B). Experimental results and density-functional theory demonstrate that the anchoring of Co single atoms on the VN surface can lower the position of V -3d at the center of the d-band of Co-VN (Figure 9C), which facilitates the desorption of OH species as well as the dissociation of water molecules (Figure 9D,E). Thanks to the improved HER kinetics, the Co-VN can reach a current density of  $10 \text{ mA}\cdot\text{cm}^{-2}$  for HER with an overpotential of only 59 mV [125]. Researchers have also found that the metal monomer Ni can optimize the hydrogen adsorption-free energy of VN [126]. The construction of porous heterostructures can expose additional active sites and modulate the electronic structure of the material. r-MoC/VN electrocatalysts with heterostructures were prepared by in situ carbonization and nitridation by Pi et al. r-MoC/VN showed a three-dimensional porous structure as revealed by SEM and TEM, which is favorable for the exposure of the active sites as well as for the contact with the electrolyte. DFT calculations and XPS reveal that there is a strong electronic interaction between r-MoC and VN, which optimizes the M-H binding energy and facilitates the desorption of  $\text{H}^*$ , thus enhancing the HER performance [127]. The HER performance of representative Vanadium-based nitrides are listed in Table 4.

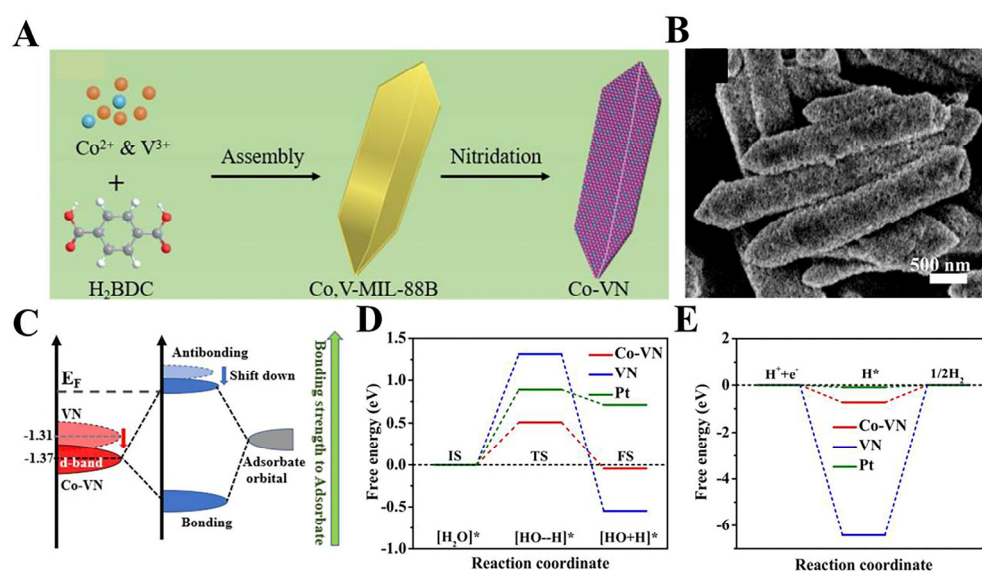


**Figure 9.** (A) Schematic illustration of the synthetic procedure of Co-VN. (B) SEM image. (C) Schematic illustration of the interaction between catalyst and adsorbate. (D) Water dissociation, and (E) H adsorption of Co-VN, VN, and Pt (1 1 1). Reproduced with permission [125]. Copyright 2023 Elsevier.

**Table 4.** Representative V-based nitrides, carbides, and phosphides for HER and OER.

Catalysts	Overpotential for HER (mV@ $10 \text{ mA cm}^{-2}$ )	Overpotential for OER (mV@ $10 \text{ mA cm}^{-2}$ )	Stability	Electrolyte	Substrate	Preparation Method	Ref.
Co-VN	59	—	60 h @ $10 \text{ mA cm}^{-2}$	1 M KOH	GCE	Gas–solid reaction	[125]
$\gamma$ -MoC/VN	86.6	—	25 h @ $60 \text{ mA cm}^{-2}$	0.5 M $\text{H}_2\text{SO}_4$	GCE	Annealing	[127]
Ni/VN	12	330	100 h @ $100 \text{ mA cm}^{-2}$	1 M KOH	NF	Gas–solid reaction	[128]
CoFe–PBAs/VN	—	290	30 h @ $10 \text{ mA cm}^{-2}$	1 M KOH	GCE	Co-precipitation	[129]
Mo, Co-VC@C	137	—	110 h @ $10 \text{ mA cm}^{-2}$	1 M KOH	GCE	Annealing	[130]



Table 4. Cont.

Catalysts	Overpotential for HER (mV@ 10 mA cm <sup>-2</sup> )	Overpotential for OER (mV@ 10 mA cm <sup>-2</sup> )	Stability	Electrolyte	Substrate	Preparation Method	Ref.
Al-VC@C	97	—	60 h @ 20 mA cm <sup>-2</sup>	1 M KOH	NF	Gas–solid reaction	[131]
VC/NC	76	—	45 h @ 20 mA cm <sup>-2</sup>	0.5 M H <sub>2</sub> SO <sub>4</sub>	GCE	Magnesiumthermic reduction	[132]
V <sub>8</sub> C <sub>7</sub> /CoP	119	290	10 h @ 10 mA cm <sup>-2</sup>	1 M KOH	CC	Gas–solid reaction	[133]
Fe <sub>x</sub> V <sub>y</sub> -PC	66	201	24 h @ 10 mA cm <sup>-2</sup>	1 M KOH	NF	Gas–solid reaction	[134]
CoVP	77	290	—	1 M KOH	CC	Gas–solid reaction	[135]
MC-V-CoP	112	—	20 h @ 10 mA cm <sup>-2</sup>	1 M PBS	GCE	Electrospinning Annealing	[136]
Co-VO <sub>x</sub> -P	230	—	24 h @ 30 mA cm <sup>-2</sup>	1 M KOH	NF	Gas–solid reaction	[137]

### 3.5.2. OER Performance

VN plays two main roles in the field of the OER: one is to be compounded with other electrocatalysts as a precatalyst to generate amorphous hydroxides or oxides as OER active species. Yang et al. synthesized VN-Co-P by hydrothermal and high-temperature nitrating. The TEM of the samples after the OER test showed amorphous mixed hydroxides and oxides, suggesting that VN itself is not really acting as an OER active species, but only as a precatalyst [138].

On the other hand, the high conductivity of VN is utilized as a carrier for other OER-active species. For example, Meng et al. grew CoFe-PBA in situ on the surface of highly conductive vanadium nitride (VN) particles by a facile co-precipitation method. CoFe-PBAs/VN hybridization improves the poor conductivity of pure CoFe-PBAs and due to the electronic interactions increases the active site of Co<sup>2+</sup> (Figure 10A). Compared to bare CoFe-PBAs (Figure 10B,C), CoFe-PBAs/VNs exhibited significantly enhanced electrocatalytic activity towards OER (a lower overpotential of 290 mV at 10 mA cm<sup>-2</sup> current density with a smaller Tafel slope of 39.72 mV dec<sup>-1</sup>) [129]. The OER performance of representative Vanadium-based nitrides are listed in Table 4.

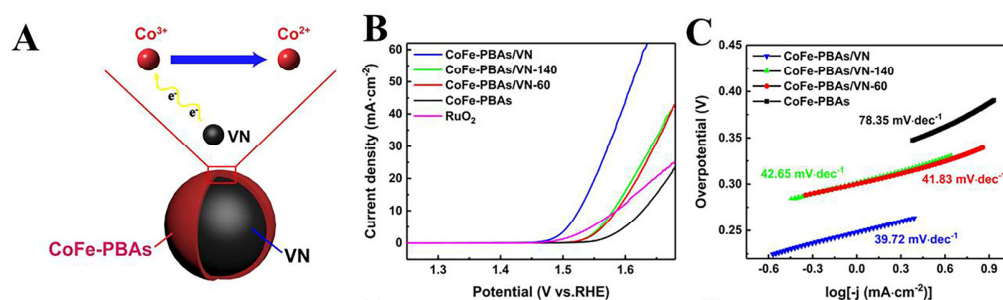


**Figure 10.** (A) Schematic diagram of electronic interaction between CoFe-PBAs and VN in CoFe-PBAs/VN. (B) LSV curves and (C) Tafel plots of RuO<sub>2</sub>, CoFe-PBAs, CoFe-PBAs/VN-60, CoFe-PBAs/VN-140, and CoFe-PBAs/VN. Reproduced with permission [129]. Copyright 2020 Elsevier.

### 3.6. Vanadium-Based Carbides

Vanadium-based carbides, as transition metal carbides, have unique metal-like properties, making the limited electron transfer from the catalyst body to the surface possible. In addition, they have the advantages of wide pH range suitability and corrosion resistance. The main vanadium-based carbides reported so far are VC, V<sub>4</sub>C<sub>3</sub>, and V<sub>8</sub>C<sub>7</sub> [139–142]. VC, V<sub>4</sub>C<sub>3</sub>, and V<sub>8</sub>C<sub>7</sub> exhibit excellent HER performance but significantly poor OER performance according to the calculation results [142]. Therefore, there is a great challenge to develop a

bifunctional vanadium-based carbide electrocatalyst for overall water splitting. The performance in the HER and OER, as well as the modification strategies, of vanadium-based carbons are presented below.

### 3.6.1. HER Performance

Some calculations have shown that  $V_8C_7$  with natural carbon vacancies has the best hydrogen precipitation ability due to its larger surface energy and appropriate hydrogen adsorption energy compared with VC and  $V_4C_3$  [142]. However, VCs are currently receiving significantly more research and attention as HER electrocatalysts. It has been shown that the interaction of VC with reaction intermediates can be effectively improved by doping engineering. Zheng et al. prepared Al-VC@C/NF for the first time by chemical vapor carbonization for efficient electrocatalytic hydrogen production (Figure 11A), which required only the overpotential of 97 mV in 1 M KOH to reach the current density of  $10 \text{ mA cm}^{-2}$ . As shown in Figure 11B–D, theoretical calculations indicate that the doped Al atoms can induce electron redistribution on the vanadium carbide surface to form electron-rich carbon sites, which significantly reduces the energy barrier for the HER [131].

Although doping engineering can improve intrinsic activity by changing the electronic structure of vanadium-based carbons, it should be noted that vanadium-based carbons inevitably agglomerate during the preparation of vanadium-based carbons, which reduces their electrocatalytic activity. Therefore, modulating the morphology of vanadium-based carbons to prepare ultrafine vanadium-based carbons is an effective way to improve the HER performance. Peng et al. synthesized vanadium carbide nanodots with a size of 7.5 nm anchored on N-doped carbon nanosheets (VC/NC) by magnesiothermic reduction (MTR). The VC/NC only acquired 76 mV to obtain the current density of  $10 \text{ mA cm}^{-2}$  in 0.5 M  $H_2SO_4$  [132]. The HER performance of representative Vanadium-based carbides are listed in Table 4.

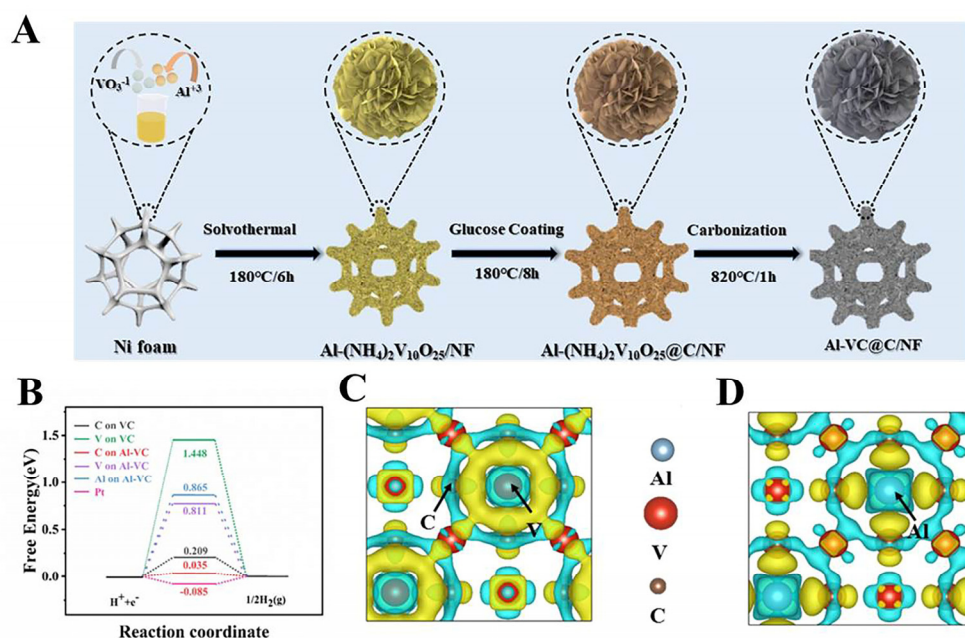


**Figure 11.** (A) Illustration of the synthesis process of Al-VC@C/NF. (B) Free energy diagram for HER of VC and Al-VC. (C,D) Charge density differences of VC and Al-VC. Reproduced with permission [131]. Copyright 2024 Elsevier.

### 3.6.2. OER Performance

It is well known that crystal surface exposure is an important factor affecting electrocatalytic performance. Kawashima et al. investigated the morphology and crystal surface exposure of cubic symmetric  $V_8C_7$  after different electrochemical CV cycling tests using it

as a precatalyst. Theoretical and experimental results indicate that the (100), (010), and (001) surfaces of  $V_8C_7$  are stable during the OER process, whereas the (110) and (111) surfaces undergo autoxidation and dissolution during the OER. This leads to the transformation of  $V_8C_7$  particle morphology from distorted spheres to cubes [143]. Constructing a heterogeneous structure can optimize the electron distribution of the material, which in turn improves the adsorption/desorption behavior of the material towards intermediates. Wu et al. prepared  $V_8C_7/CoP$  composites by hydrothermal and solid-phase phosphatization, which required only 290 mV overpotential to achieve a current density of  $10 \text{ mA cm}^{-2}$  in 1 M KOH due to the synergistic interaction between  $V_8C_7$  and CoP [133]. The OER performance of representative Vanadium-based carbides are listed in Table 4.

### 3.7. Vanadium-Based Phosphides

Transition metal phosphides (TMPs) have good electrical conductivity, as well as a wide range of stoichiometric ratios and crystal shapes that can be adjusted to meet specific requirements. The positively charged metal sites and negatively charged P sites can act as hydrides and proton acceptors, respectively, to enhance HER performance [144–146]. In addition, the P-anion protects metal phosphides from being easily dissolved. So, TMPs have good stability over a wide pH range [147,148]. Recently, V-based phosphides used as representative transition metal phosphides have also received extensive attention. The following are the performance and modification strategies of vanadium-based phosphides for the HER and OER.

#### 3.7.1. HER Performance

In vanadium-based phosphides, elemental vanadium has the potential to form  $V_2P$  crystals with P or to be doped as a cation into the lattice of other metal phosphides. Suo et al. synthesized Fe-doped vanadium phosphide ( $V_2P$ ) by a two-step hydrothermal and solid-phase phosphatization method. The high valence state of V is favorable for the enhancement of the binding ability of the catalyst surface to  $H^*$  during the HER process. In addition, the morphology and conductivity of vanadium phosphides can be modified by introducing Fe doping. Thanks to these advantages,  $Fe_xV_y-PC/NF$  can reach  $10 \text{ mA cm}^{-2}$  current density in 1 M KOH with only 66 mV of overpotential [134]. Han et al. prepared vanadium-doped cobalt phosphide (CoVP) on carbon cloth, and the doping of V ions led to the optimization of the surface electronic structure of the CoP nanosheets, which required only an overpotential of 77 mV to obtain a current density of  $10 \text{ mA cm}^{-2}$  in 1 M KOH [135]. The HER performance of representative Vanadium-based phosphides are listed in Table 4.

#### 3.7.2. OER Performance

Wang et al. synthesized CoVM ( $M = P, S, \text{ and } Se$ ) catalysts with nanosphere morphology consisting of nanoneedles by one-step hydrothermal and low-temperature phosphorization. Among them, the CoVP electrode showed efficient catalytic performance for the OER, which required an overpotential of only 270 mV to acquire a current density of  $10 \text{ mA cm}^{-2}$ . The good OER performance was attributed to the fast charge transfer rate and the exposure of additional active sites by the synergistic catalytic effect of CoP and  $V_3P$ . Meanwhile, DFT calculations show that the  $V_3P$  material exhibits a higher density of states near the Fermi energy level, which enhances the conductivity of the material [149].

Zhu et al. prepared Co- $VO_x$ -P nanoflowers on nickel foam as oxygen-removing electrocatalysts and achieved a smaller overpotential of 230 mV for OER at  $100 \text{ mA cm}^{-2}$ . Experiments and DFT calculations showed that on the Co- $VO_x$ -P surface, V doping changed the d-band center of the catalyst (Figure 12A), and the chemisorption of oxygen-containing intermediates on the metal atoms was greatly weakened by V doping (Figure 12B,C). Overall, the Co- $VO_x$ -P electrocatalysts showed improved intrinsic catalytic properties enhanced conductivity, easy electron transfer, and good surface adsorption strength due to the combination of P and V. The OER performance of representative Vanadium-based phosphides are listed in Table 4. In summary, V in V-based phosphides not only improves

the electrical conductivity of the catalyst but also optimizes the intrinsic activity of the electrocatalyst by tuning the electronic structure [137].

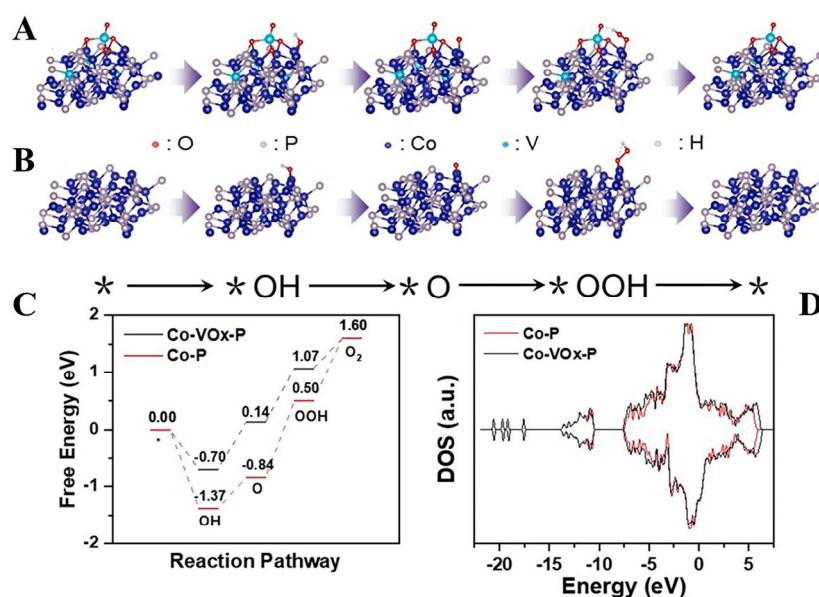


**Figure 12.** (A,B) The optimized interaction between intermediates on Co-Vox-P and Co-P surfaces for the OER. (C) The free energy diagram for each elemental step of the OER for Co-Vox-P and Co-P. (D) TDOS of Co-VO<sub>x</sub>-P and Co-P. Reproduced with permission [137]. Copyright 2022 Elsevier.

#### 4. Summary and Outlook

Vanadium-based electrocatalysts for water splitting have gained a considerable amount of attention in recent decades owing to their many benefits, such as excellent electrocatalytic performance, low cost, and adjustable electronic structure. Nevertheless, a comprehensive overview of vanadium-based electrocatalysts for water splitting is currently lacking. Thus, in this review, we firstly demonstrate the mechanisms of the HER and OER under acidic and alkaline conditions and then focus on the developments currently made in vanadium-based water-splitting electrocatalysts, including vanadium oxides, hydroxides, dichalcogenides, phosphides, nitrides, carbides, and vanadate. Despite notable developments in the research of vanadium-based electrocatalysts for the processes of the HER and OER, there are still numerous existing issues to solve. Herein, we present some valuable perspectives and suggestions on the current obstacles to V-based electrocatalysts for water splitting.

1. It is recommended that new V-based water-splitting electrocatalysts, such as V-based phosphides and carbides, are further developed, along with exploring their potential applications in seawater electrolysis. Moreover, the testing conditions for V-based water-splitting electrocatalysts in the literature are often carried out at room temperature and in 1 M KOH solutions. However, higher temperatures (60–80 °C) and more concentrated alkaline environments (30 wt% KOH or 6 M KOH) are more relevant to the actual production process. Therefore, application-related conditions should be considered to comprehensively assess their suitability in the actual production process when conducting performance tests on V-based water-splitting electrocatalysts.
2. Recent literature reports suggest that non-oxide/hydroxide V-based water-splitting electrocatalysts may act merely as precatalysts in the OER process, rather than being the true active species involved in the reaction. Therefore, it is necessary to employ a suite of in situ characterization techniques (such as in situ Raman, in situ FTIR, and in situ XPS) along with synchrotron radiation to further ascertain the actual active species of non-oxide/hydroxide V-based electrocatalysts during the OER process and to explore the role of elemental V therein.

3. Developing bifunctional V-based nitrides and sulfides as electrocatalysts for overall water splitting presents significant challenges. We have found that vanadium-based sulfides and nitrides, particularly vanadium nitrides, exhibit excellent HER performance. However, due to the sluggish reaction kinetics of the OER, their OER performance is less satisfactory. Therefore, it is necessary to further optimize the adsorption of oxygen-containing intermediates for V-based nitrides and sulfides via doping engineering, surface modification, and other strategies, aiming to boost their OER performance for efficient overall water splitting.
4. The stability of V-based electrocatalysts for the HER and OER reported so far is relatively good for small current densities. However, it is essential to recognize that the element V is soluble in aqueous electrolytes. Thus, it is essential to explore the stability of V-based electrocatalysts at high current densities. This issue can be considered from two perspectives: One is to inhibit the dissolution of V during the electrocatalysis process through carbon material encapsulation and valence engineering. Secondly, V-based water-splitting electrocatalysts with a superhydrophilic–superhydrophobic structure can be designed to prevent bubble blockage at the active sites, thereby enhancing stability.

**Author Contributions:** Writing—original draft preparation, H.L. writing—review and editing, J.W. and M.L. project administration, Y.W. All authors have read and agreed to the published version of the manuscript.

**Funding:** We gratefully acknowledge the support of this research by the National Natural Science Foundation of China (No. 61761047 and 41876055), Yunnan University’s Practical Innovation Fund for Graduate Students (ZC-23234859), and the Program for Innovative Research Team (in Science and Technology) in the University of Yunnan Province.

**Data Availability Statement:** No new data were created or analyzed in this study. Data sharing is not applicable to this article.

**Conflicts of Interest:** The authors declare no conflicts of interest.

## References

1. Zhou, W.; Li, X.; Li, X.; Shao, J.; Yang, H.; Chai, X.; Hu, Q.; He, C. Crafting amorphous VO<sub>2</sub>–crystalline NiS<sub>2</sub> heterostructures as bifunctional electrocatalysts for efficient water splitting: The different cocatalytic function of VO<sub>2</sub>. *Chem. Eng. J.* **2023**, *470*, 144146. [[CrossRef](#)]
2. Wang, S.; Sun, L.; Iqbal, S. Green financing role on renewable energy dependence and energy transition in E7 economies. *Renew. Energy* **2022**, *200*, 1561–1572. [[CrossRef](#)]
3. Ameer, W.; Ali, M.S.e.; Farooq, F.; Ayub, B.; Waqas, M. Renewable energy electricity, environmental taxes, and sustainable development: Empirical evidence from E7 economies. *Environ. Sci. Pollut. Res.* **2023**. [[CrossRef](#)]
4. Song, W.; Li, M.; Wang, C.; Lu, X. Electronic modulation and interface engineering of electrospun nanomaterials-based electrocatalysts toward water splitting. *Carbon Energy* **2021**, *3*, 101–128. [[CrossRef](#)]
5. Pan, S.; Ma, Z.; Yang, W.; Dongyang, B.; Yang, H.; Lai, S.; Dong, F.; Yang, X.; Lin, Z. Magnesium incorporation activates perovskite cobaltites toward efficient and stable electrocatalytic oxygen evolution. *Mater. Rep. Energy* **2023**, *3*, 100212. [[CrossRef](#)]
6. Sun, H.; Xu, X.; Kim, H.; Shao, Z.; Jung, W. Advanced electrocatalysts with unusual active sites for electrochemical water splitting. *InfoMat* **2024**, *6*, e12494. [[CrossRef](#)]
7. Xu, X.; Zhou, Q.; Yu, D. The future of hydrogen energy: Bio-hydrogen production technology. *Int. J. Hydrogen Energy* **2022**, *47*, 33677–33698. [[CrossRef](#)]
8. Terlouw, T.; Bauer, C.; McKenna, R.; Mazzotti, M. Large-scale hydrogen production via water electrolysis: A techno-economic and environmental assessment. *Energy Environ. Sci.* **2022**, *15*, 3583–3602. [[CrossRef](#)]
9. Panchenko, V.A.; Daus, Y.V.; Kovalev, A.A.; Yudaev, I.V.; Litt, Y.V. Prospects for the production of green hydrogen: Review of countries with high potential. *Int. J. Hydrogen Energy* **2023**, *48*, 4551–4571. [[CrossRef](#)]
10. Li, H.; Xiao, Y.; Tian, X.; Xing, X.; Cao, M.; Wang, Y. A crystalline/amorphous FeCo alloy/FeCoNi-Pi bifunctional electrocatalyst for efficient overall water splitting. *Inorg. Chem. Front.* **2024**. [[CrossRef](#)]
11. Sonadia; Iqbal, Z.; Miran, W.; Ul-Hamid, A.; Ayub, K.S.; Azad, F. Enhanced Electrocatalytic Performance of Erbium-Incorporated Nickel-Based Metal–Organic Frameworks for Water Splitting. *Energy Fuels* **2024**, *38*, 5397–5406. [[CrossRef](#)]
12. Yue, D.; Feng, T.; Zhu, Z.; Lu, S.; Yang, B. Ir Single Atom-Doped Ni<sub>2</sub>P Anchored by Carbonized Polymer Dots for Robust Overall Water Splitting. *ACS Catal.* **2024**, *14*, 3006–3017. [[CrossRef](#)]

13. Mohili, R.; Hemanth, N.R.; Jin, H.; Lee, K.; Chaudhari, N. Emerging high entropy metal sulphides and phosphides for electrochemical water splitting. *J. Mater. Chem. A* **2023**, *11*, 10463–10472. [[CrossRef](#)]
14. Wang, J.; Yang, H.; Li, F.; Li, L.; Wu, J.; Liu, S.; Cheng, T.; Xu, Y.; Shao, Q.; Huang, X. Single-site Pt-doped RuO<sub>2</sub> hollow nanospheres with interstitial C for high-performance acidic overall water splitting. *Sci. Adv.* **2022**, *8*, eabl9271. [[CrossRef](#)]
15. Nicole, S.L.D.; Li, Y.; Xie, W.; Wang, G.; Lee, J.-M. Heterointerface and Tensile Strain Effects Synergistically Enhances Overall Water-Splitting in Ru/RuO<sub>2</sub> Aerogels. *Small* **2023**, *19*, 2206844. [[CrossRef](#)]
16. Wang, N.; Ning, S.; Yu, X.; Chen, D.; Li, Z.; Xu, J.; Meng, H.; Zhao, D.; Li, L.; Liu, Q.; et al. Graphene composites with Ru-RuO<sub>2</sub> heterostructures: Highly efficient Mott–Schottky-type electrocatalysts for pH-universal water splitting and flexible zinc–air batteries. *Appl. Catal. B* **2022**, *302*, 120838. [[CrossRef](#)]
17. Yao, Q.; Huang, B.; Zhang, N.; Sun, M.; Shao, Q.; Huang, X. Channel-Rich RuCu Nanosheets for pH-Universal Overall Water Splitting Electrocatalysis. *Angew. Chem. Int. Ed.* **2019**, *58*, 13983–13988. [[CrossRef](#)]
18. Batool, M.; Hameed, A.; Nadeem, M.A. Recent developments on iron and nickel-based transition metal nitrides for overall water splitting: A critical review. *Coord. Chem. Rev.* **2023**, *480*, 215029. [[CrossRef](#)]
19. Sabir, A.S.; Pervaiz, E.; Khosa, R.; Sohail, U. An inclusive review and perspective on Cu-based materials for electrochemical water splitting. *RSC Adv.* **2023**, *13*, 4963–4993. [[CrossRef](#)]
20. Li, J.; Tang, C.; Zhang, H.; Zou, Z.; Li, C.M. Mesoporous molybdenum carbide for greatly enhanced hydrogen evolution at high current density and its mechanism studies. *Mater. Rep. Energy* **2023**, *3*, 100215. [[CrossRef](#)]
21. Abdelghafar, F.; Xu, X.; Jiang, S.P.; Shao, Z. Perovskite for Electrocatalytic Oxygen Evolution at Elevated Temperatures. *ChemSusChem* **2024**, e202301534. [[CrossRef](#)]
22. Han, Y.H.; Lee, S.H.; Kim, K.T.; Choi, I.H.; Moon, S. Properties of Electrical Conductivity of Amorphous Tungsten-Doped Vanadium Oxide for Uncooled Microbolometers. *Solid State Phenom.* **2007**, *124–126*, 343–346. [[CrossRef](#)]
23. Carrero, C.A.; Schloegl, R.; Wachs, I.E.; Schomaecker, R. Critical Literature Review of the Kinetics for the Oxidative Dehydrogenation of Propane over Well-Defined Supported Vanadium Oxide Catalysts. *ACS Catal.* **2014**, *4*, 3357–3380. [[CrossRef](#)]
24. Kim, Y.; Park, Y.; Kim, M.; Lee, J.; Kim, K.J.; Choi, J.W. Corrosion as the origin of limited lifetime of vanadium oxide-based aqueous zinc ion batteries. *Nat. Commun.* **2022**, *13*, 2371. [[CrossRef](#)]
25. Zhu, J.; Chen, X.; Thang, A.Q.; Li, F.-L.; Chen, D.; Geng, H.; Rui, X.; Yan, Q. Vanadium-based metal-organic frameworks and their derivatives for electrochemical energy conversion and storage. *SmartMat* **2022**, *3*, 384–416. [[CrossRef](#)]
26. Wu, C.; Zhong, M.; Tan, Y. Highly efficient and stable vanadium-based electrocatalysts: Stoichiometric iron vanadium sulfides for water-oxidation at large current densities. *Chem. Eng. J.* **2023**, *477*, 146981. [[CrossRef](#)]
27. Ehsan, M.A.; Khan, A.; Al-Ahmed, A.; Hakeem, A.S.; Afzaal, M.; Pandey, S.; Mahar, N. Aerosol-assisted chemical vapour deposited vanadium oxide thin films on nickel foam with auspicious electrochemical water oxidation properties. *Int. J. Hydrogen Energy* **2024**, *52*, 718–727. [[CrossRef](#)]
28. Ma, Y.; Li, M.-X.; Luan, R.-N.; Li, C.-R.; Liu, X.; Zhao, H.-Y.; Wang, Y.-H.; Chai, Y.-M.; Dong, B. Scalloped nickel/iron vanadium oxide-coated vanadium dioxides based on chemical etching-induced reconstruction strategy for efficient oxygen evolution. *Int. J. Hydrogen Energy* **2022**, *47*, 33352–33360. [[CrossRef](#)]
29. Gonçalves, J.M.; Martins, P.R.; Araki, K.; Angnes, L. Recent progress in water splitting and hybrid supercapacitors based on nickel-vanadium layered double hydroxides. *J. Energy Chem.* **2021**, *57*, 496–515. [[CrossRef](#)]
30. Yang, M.; Shang, C.; Li, F.; Liu, C.; Wang, Z.; Gu, S.; Liu, D.; Cao, L.; Zhang, J.; Lu, Z.; et al. Synergistic electronic and morphological modulation on ternary Co<sub>1-x</sub>V<sub>x</sub>P nanoneedle arrays for hydrogen evolution reaction with large current density. *Sci. China Mater.* **2021**, *64*, 880–891. [[CrossRef](#)]
31. Li, Z.; Li, B.; Yu, M.; Yu, C.; Shen, P. Amorphous metallic ultrathin nanostructures: A latent ultra-high-density atomic-level catalyst for electrochemical energy conversion. *Int. J. Hydrogen Energy* **2022**, *47*, 26956–26977. [[CrossRef](#)]
32. Wu, Z.-P.; Lu, X.F.; Zang, S.-Q.; Lou, X.W. Non-Noble-Metal-Based Electrocatalysts toward the Oxygen Evolution Reaction. *Adv. Funct. Mater.* **2020**, *30*, 1910274. [[CrossRef](#)]
33. Xu, H.; Yuan, J.; He, G.; Chen, H. Current and future trends for spinel-type electrocatalysts in electrocatalytic oxygen evolution reaction. *Coord. Chem. Rev.* **2023**, *475*, 214869. [[CrossRef](#)]
34. Kashif, M.; Thangarasu, S.; Murugan, N.; Magdum, S.S.; Kim, Y.A.; Kurkuri, M.; Oh, T.-H. Interatomic interaction of 2D crumpled V<sub>2</sub>O<sub>5</sub> nanosheets layered with Ni-MOF as a bifunctional electrocatalyst for overall water splitting and supercapacitor applications. *J. Energy Storage* **2024**, *81*, 110348. [[CrossRef](#)]
35. Ha, Q.-N.; Yeh, C.-H.; Gultom, N.S.; Kuo, D.-H. Industrial-scale efficient alkaline water electrolysis achieved with sputtered NiFeV-oxide thin film electrodes for green hydrogen production. *J. Mater. Chem. A* **2024**, *12*, 460–474. [[CrossRef](#)]
36. Zhou, P.; Lv, X.; Gao, Y.; Cui, Z.; Liu, Y.; Wang, Z.; Wang, P.; Zheng, Z.; Dai, Y.; Huang, B. Enhanced electrocatalytic HER performance of non-noble metal nickel by introduction of divanadium trioxide. *Electrochim. Acta* **2019**, *320*, 134535. [[CrossRef](#)]
37. Liu, G.; Lv, H.; Quan, Q.; Li, X.; Lu, H.; Li, W.; Cui, X.; Jiang, L. Self-powered electrolysis systems for sustainable hydrogen generation from natural seawater via a Ni/V<sub>2</sub>O<sub>3</sub> Schottky electrode. *Chem. Eng. J.* **2022**, *450*, 138079. [[CrossRef](#)]
38. Fan, X.-Z.; Pang, Q.-Q.; Fan, F.; Yao, H.-C.; Li, Z.-J. Ultra-fine Ru nanoparticles decorated V<sub>2</sub>O<sub>3</sub> as a pH-universal electrocatalyst for efficient hydrogen evolution reaction. *Int. J. Hydrogen Energy* **2023**, *48*, 20577–20587. [[CrossRef](#)]

39. Li, D.; Wang, J.; Wang, S.; Chu, B.; Li, R.; Li, B.; Dong, L.; Fan, M.; Chen, Z. An interface engineering induced hierarchical NiCo/V<sub>2</sub>O<sub>3</sub>/C Schottky heterojunction catalyst for large-current-density hydrogen evolution reaction. *J. Mater. Chem. A* **2023**, *11*, 23397–23404. [[CrossRef](#)]
40. Lee, S.; Ivanov, I.N.; Keum, J.K.; Lee, H.N. Epitaxial stabilization and phase instability of VO<sub>2</sub> polymorphs. *Sci. Rep.* **2016**, *6*, 19621. [[CrossRef](#)]
41. Shao, Z.; Cao, X.; Luo, H.; Jin, P. Recent progress in the phase-transition mechanism and modulation of vanadium dioxide materials. *NPG Asia Mater.* **2018**, *10*, 581–605. [[CrossRef](#)]
42. Kim, K.-H.; Kim, K.-H.; Choi, W.; Kim, Y.-M.; Hong, S.-H.; Choi, Y.-H. Mapping the electrocatalytic water splitting activity of VO<sub>2</sub> across its insulator-to-metal phase transition. *Nanoscale* **2022**, *14*, 8281–8290. [[CrossRef](#)]
43. Haldar, K.K.; Ahmed, I.; Biswas, R.; Mete, S.; Patil, R.A.; Ma, Y.-R. Efficient MoS<sub>2</sub>/V<sub>2</sub>O<sub>5</sub> Electrocatalyst for Enhanced Oxygen and Hydrogen Evolution Reactions. *Electrocatalysis* **2023**, *14*, 624–635. [[CrossRef](#)]
44. Zhong, X.; Zhang, L.; Tang, J.; Chai, J.; Xu, J.; Cao, L.; Yang, M.; Yang, M.; Kong, W.; Wang, S.; et al. Efficient coupling of a hierarchical V<sub>2</sub>O<sub>5</sub>@Ni<sub>3</sub>S<sub>2</sub> hybrid nanoarray for pseudocapacitors and hydrogen production. *J. Mater. Chem. A* **2017**, *5*, 17954–17962. [[CrossRef](#)]
45. Wu, J.; Qin, X.; Xia, Y.; Zhang, Y.; Zhang, B.; Du, Y.; Wang, H.-L.; Li, S.; Xu, P. Surface oxidation protection strategy of CoS<sub>2</sub> by V<sub>2</sub>O<sub>5</sub> for electrocatalytic hydrogen evolution reaction. *Nanoscale Horiz.* **2023**, *8*, 338–345. [[CrossRef](#)]
46. Tang, J.; Ruan, Q.; Yu, H.; Huang, C. Activating Co(OH)<sub>2</sub> Active Sites by Coupled with V<sub>2</sub>O<sub>5</sub> to Boost Highly Efficient Oxygen Evolution Reaction. *Adv. Sustain. Syst.* **2023**, *7*, 2200473. [[CrossRef](#)]
47. Pu, Y.; Liu, Y.; Tang, X.; Huang, Q.; Huang, L. Fast and in situ releasing of active species confined in two-dimensional layers for superior overall electrochemical water splitting. *Appl. Catal. B* **2024**, *341*, 123319. [[CrossRef](#)]
48. He, D.; Cao, L.; Huang, J.; Kajiyoshi, K.; Wu, J.; Wang, C.; Liu, Q.; Yang, D.; Feng, L. In-situ optimizing the valence configuration of vanadium sites in NiV-LDH nanosheet arrays for enhanced hydrogen evolution reaction. *J. Energy Chem.* **2020**, *47*, 263–271. [[CrossRef](#)]
49. Li, W.; Feng, B.; Yi, L.; Li, J.; Hu, W. Highly Efficient Alkaline Water Splitting with Ru-Doped Co–V Layered Double Hydroxide Nanosheets as a Bifunctional Electrocatalyst. *ChemSusChem* **2021**, *14*, 730–737. [[CrossRef](#)]
50. De, A.; Madhu, R.; Bera, K.; Dhandapani, H.N.; Nagappan, S.; Singha Roy, S.; Kundu, S. Deciphering the amplification of dual catalytic active sites of Se-doped NiV LDH in water electrolysis: A hidden gem exposure of anion doping at the core-lattice LDH framework. *J. Mater. Chem. A* **2023**, *11*, 25055–25071. [[CrossRef](#)]
51. Zhu, Y.-X.; Liu, M.; Hou, G.-Y.; Tang, Y.-P.; Wu, L.-K. The release of metal ions induced surface reconstruction of layered double hydroxide electrocatalysts. *Sustain. Energy Fuels* **2021**, *5*, 3436–3444. [[CrossRef](#)]
52. Xu, L.; Yuan, B.; Min, L.; Xu, W.; Zhang, W. Preparation of NiCo-LDH@NiCoV-LDH interconnected nanosheets as high-performance electrocatalysts for overall water splitting. *Int. J. Hydrogen Energy* **2022**, *47*, 15583–15592. [[CrossRef](#)]
53. Srividhya, G.; Sangavi, T.; Viswanathan, C.; Ponpandian, N. Cobalt–Iron Co-substituted NiV Layered Double Hydroxide as a High-Performance Electrocatalyst for Oxygen Evolution Reaction in a Neutral Saline Medium. *ACS Appl. Energy Mater.* **2024**, *7*, 154–164. [[CrossRef](#)]
54. Maji, M.; Dihingia, N.; Dutta, S.; Parvin, S.; Pati, S.K.; Bhattacharyya, S. Charge transfer modulated heterointerfaces for hydrogen production at all pH values. *J. Mater. Chem. A* **2022**, *10*, 24927–24937. [[CrossRef](#)]
55. Liu, Q.; Huang, J.; Zhao, Y.; Cao, L.; Li, K.; Zhang, N.; Yang, D.; Feng, L.; Feng, L. Tuning the coupling interface of ultrathin Ni<sub>3</sub>S<sub>2</sub>@NiV-LDH heterogeneous nanosheet electrocatalysts for improved overall water splitting. *Nanoscale* **2019**, *11*, 8855–8863. [[CrossRef](#)]
56. Najafi, L.; Oropesa-Nuñez, R.; Bellani, S.; Martín-García, B.; Pasquale, L.; Serri, M.; Drago, F.; Luxa, J.; Sofer, Z.; Sedmidubský, D.; et al. Topochemical Transformation of Two-Dimensional VSe<sub>2</sub> into Metallic Nonlayered VO<sub>2</sub> for Water Splitting Reactions in Acidic and Alkaline Media. *ACS Nano* **2022**, *16*, 351–367. [[CrossRef](#)]
57. Jiang, J.; Sun, F.; Zhou, S.; Hu, W.; Zhang, H.; Dong, J.; Jiang, Z.; Zhao, J.; Li, J.; Yan, W.; et al. Atomic-level insight into super-efficient electrocatalytic oxygen evolution on iron and vanadium co-doped nickel (oxy)hydroxide. *Nat. Commun.* **2018**, *9*, 2885. [[CrossRef](#)]
58. Karmakar, A.; Karthick, K.; Sankar, S.S.; Kumaravel, S.; Madhu, R.; Bera, K.; Dhandapani, H.N.; Nagappan, S.; Murugan, P.; Kundu, S. Stabilization of ruthenium nanoparticles over NiV-LDH surface for enhanced electrochemical water splitting: An oxygen vacancy approach. *J. Mater. Chem. A* **2022**, *10*, 3618–3632. [[CrossRef](#)]
59. Lv, J.; Liu, P.; Li, R.; Wang, L.; Zhang, K.; Zhou, P.; Huang, X.; Wang, G. Constructing accelerated charge transfer channels along V-Co-Fe via introduction of V into CoFe-layered double hydroxides for overall water splitting. *Appl. Catal. B* **2021**, *298*, 120587. [[CrossRef](#)]
60. Guan, J.; Li, X.; Zhu, Y.; Dai, Y.; Zhang, R.; Guo, B.; Zhang, M. Ni<sub>5</sub>P<sub>4</sub>-embedded FeV LDH porous nanosheets for enhancing oxygen evolution and urea oxidation reactions. *New J. Chem.* **2023**, *47*, 16964–16971. [[CrossRef](#)]
61. Wan, X.; Song, Y.; Zhou, H.; Shao, M. Layered Double Hydroxides for Oxygen Evolution Reaction towards Efficient Hydrogen Generation. *Energy Mater. Adv.* **2022**, *2022*, 9842610. [[CrossRef](#)]
62. Laipan, M.; Yu, J.; Zhu, R.; Zhu, J.; Smith, A.T.; He, H.; O'Hare, D.; Sun, L. Functionalized layered double hydroxides for innovative applications. *Mater. Horiz.* **2020**, *7*, 715–745. [[CrossRef](#)]

63. Gonçalves, J.M.; Ireno da Silva, M.; Angnes, L.; Araki, K. Vanadium-containing electro and photocatalysts for the oxygen evolution reaction: A review. *J. Mater. Chem. A* **2020**, *8*, 2171–2206. [[CrossRef](#)]
64. Ansari, M.S.; Kim, H. Enhanced electrocatalytic oxygen evolution reaction kinetics using dual-phase engineering of self-supported hierarchical NiCoV(OH)<sub>x</sub> nanowire arrays. *Fuel* **2021**, *304*, 121309. [[CrossRef](#)]
65. Zeng, K.; Tian, M.; Chen, X.; Zhang, J.; Rummeli, M.H.; Strasser, P.; Sun, J.; Yang, R. Strong electronic coupling between single Ru atoms and cobalt-vanadium layered double hydroxide harness efficient water splitting. *Chem. Eng. J.* **2023**, *452*, 139151. [[CrossRef](#)]
66. Zhang, B.; Wu, Z.; Shao, W.; Gao, Y.; Wang, W.; Ma, T.; Ma, L.; Li, S.; Cheng, C.; Zhao, C. Interfacial Atom-Substitution Engineered Transition-Metal Hydroxide Nanofibers with High-Valence Fe for Efficient Electrochemical Water Oxidation. *Angew. Chem. Int. Ed.* **2022**, *61*, e202115331. [[CrossRef](#)]
67. Nejati, K.; Akbari, A.R.; Davari, S.; Asadpour-Zeynali, K.; Rezvani, Z. Zn-Fe-layered double hydroxide intercalated with vanadate and molybdate anions for electrocatalytic water oxidation. *New J. Chem.* **2018**, *42*, 2889–2895. [[CrossRef](#)]
68. Yang, Z.; Chen, H.; Xiang, M.; Yu, C.; Hui, J.; Dong, S. Coral reef structured cobalt-doped vanadate oxometalate nanoparticle for a high-performance electrocatalyst in water splitting. *Int. J. Hydrogen Energy* **2022**, *47*, 31566–31574. [[CrossRef](#)]
69. Yang, Z.; Fan, W.; Zhang, P.; Zhuang, H.; Xiang, M.; Hui, J. Ni<sub>2</sub>V<sub>2</sub>O<sub>7</sub> dandelion microsphere for a high-performance electrocatalyst in water splitting. *Int. J. Hydrogen Energy* **2021**, *46*, 39658–39664. [[CrossRef](#)]
70. Guo, W.; Yang, T.; Zhang, H.; Zhou, H.; Wei, W.; Liang, W.; Zhou, Y.; Yu, T.; Zhao, H. Charge-counterbalance modulated amorphous nickel oxide for efficient alkaline hydrogen and oxygen evolution. *Chem. Eng. J.* **2023**, *470*, 144241. [[CrossRef](#)]
71. Pan, M.; Qian, G.; Yu, T.; Chen, J.; Luo, L.; Zou, Y.; Yin, S. Ni modified Co<sub>2</sub>VO<sub>4</sub> heterojunction with poor/rich-electron structure for overall urea-rich wastewater oxidation. *Chem. Eng. J.* **2022**, *435*, 134986. [[CrossRef](#)]
72. Zhou, Y.; Wu, Y.; Guo, D.; Li, J.; Chu, D.; Na, S.; Yu, M.; Li, D.; Sui, G.; Chai, D.-F. Anchoring metal-organic framework-derived hollow CoV<sub>2</sub>O<sub>6</sub> nanocubes onto lattice tensile strained V<sub>2</sub>CT<sub>x</sub> MXene for superior overall water splitting. *J. Alloys Compd.* **2023**, *963*, 171133. [[CrossRef](#)]
73. Pan, M.; Chen, W.; Qian, G.; Yu, T.; Wang, Z.; Luo, L.; Yin, S. Carbon-encapsulated Co<sub>3</sub>V decorated Co<sub>2</sub>VO<sub>4</sub> nanosheets for enhanced urea oxidation and hydrogen evolution reaction. *Electrochim. Acta* **2022**, *407*, 139882. [[CrossRef](#)]
74. Luo, Z.; Peng, Q.; Huang, Z.; Wang, L.; Yang, Y.; Dong, J.; Isimjan, T.T.; Yang, X. Fine-tune d-band center of cobalt vanadium oxide nanosheets by N-doping as a robust overall water splitting electrocatalyst. *J. Colloid Interface Sci.* **2023**, *629*, 111–120. [[CrossRef](#)]
75. Gyanprakash, D.M.; Sharma, G.P.; Gupta, P.K. Isovalent anion-induced electrochemical activity of doped Co<sub>3</sub>V<sub>2</sub>O<sub>8</sub> for oxygen evolution reaction application. *Dalton Trans.* **2022**, *51*, 15312–15321. [[CrossRef](#)]
76. Li, A.; Tang, X.; Cao, R.; Song, D.; Wang, F.; Yan, H.; Chen, H.; Wei, Z. Directed Surface Reconstruction of Fe Modified Co<sub>2</sub>VO<sub>4</sub> Spinel Oxides for Water Oxidation Catalysts Experiencing Self-Terminating Surface Deterioration. *Adv. Mater.* **2024**, 2401818. [[CrossRef](#)]
77. Ma, H.; Sun, C.; Wang, Z.; Jiang, Q. Tuning the electronic structure of NiCoVO<sub>x</sub> nanosheets through S doping for enhanced oxygen evolution. *Nanoscale* **2021**, *13*, 17022–17027. [[CrossRef](#)]
78. Xu, Q.; Qin, W.; Chu, J.-F. Novel Co<sub>3(1-x)</sub>Fe<sub>3x</sub>V<sub>2</sub>O<sub>8</sub> Nanoparticles as Highly Active and Noble-Metal-Free Electrocatalysts for Oxygen Evolution Reaction. *Energy Fuels* **2020**, *34*, 15019–15025. [[CrossRef](#)]
79. Mondal, A.; Ganguli, S.; Inta, H.R.; Mahalingam, V. Influence of Vanadate Structure on Electrochemical Surface Reconstruction and OER Performance of CoV<sub>2</sub>O<sub>6</sub> and Co<sub>3</sub>V<sub>2</sub>O<sub>8</sub>. *ACS Appl. Energy Mater.* **2021**, *4*, 5381–5387. [[CrossRef](#)]
80. Li, Q.; Zhang, X.; Shen, J.; Ji, X.; Liu, J. Bifunctional keel flower-like Ni-Co-V multicomponent oxide catalyst with enhanced electron transport for accelerating overall water splitting. *J. Colloid Interface Sci.* **2022**, *628*, 467–476. [[CrossRef](#)]
81. Aftab, S.; Iqbal, M.Z.; Rim, Y.S. Recent Advances in Rolling 2D TMDs Nanosheets into 1D TMDs Nanotubes/Nanoscrolls. *Small* **2023**, *19*, 2205418. [[CrossRef](#)]
82. Tang, X.; Hao, Q.; Hou, X.; Lan, L.; Li, M.; Yao, L.; Zhao, X.; Ni, Z.; Fan, X.; Qiu, T. Exploring and Engineering 2D Transition Metal Dichalcogenides toward Ultimate SERS Performance. *Adv. Mater.* **2024**, *36*, 2312348. [[CrossRef](#)]
83. Sanap, P.P.; Gupta, S.P.; Kahandal, S.S.; Gunjekar, J.L.; Lokhande, C.D.; Sankapal, B.R.; Said, Z.; Bulakhe, R.N.; Man Kim, J.; Bhalerao, A.B. Exploring vanadium-chalcogenides toward solar cell application: A review. *J. Ind. Eng. Chem.* **2024**, *129*, 124–142. [[CrossRef](#)]
84. Yuan, J.; Wu, J.; Hardy, W.J.; Loya, P.; Lou, M.; Yang, Y.; Najmaei, S.; Jiang, M.; Qin, F.; Keyshar, K.; et al. Facile Synthesis of Single Crystal Vanadium Disulfide Nanosheets by Chemical Vapor Deposition for Efficient Hydrogen Evolution Reaction. *Adv. Mater.* **2015**, *27*, 5605–5609. [[CrossRef](#)]
85. Feng, J.; Sun, X.; Wu, C.; Peng, L.; Lin, C.; Hu, S.; Yang, J.; Xie, Y. Metallic Few-Layered VS<sub>2</sub> Ultrathin Nanosheets: High Two-Dimensional Conductivity for In-Plane Supercapacitors. *J. Am. Chem. Soc.* **2011**, *133*, 17832–17838. [[CrossRef](#)]
86. Karthick, K.; Bijoy, T.K.; Sivakumaran, A.; Mansoor Basha, A.B.; Murugan, P.; Kundu, S. Enhancing Hydrogen Evolution Reaction Activities of 2H-Phase VS<sub>2</sub> Layers with Palladium Nanoparticles. *Inorg. Chem.* **2020**, *59*, 10197–10207. [[CrossRef](#)]
87. Hussain, S.; Vikraman, D.; Sarfraz, M.; Faizan, M.; Patil, S.A.; Batoo, K.M.; Nam, K.-W.; Kim, H.-S.; Jung, J. Design of XS<sub>2</sub> (X = W or Mo)-Decorated VS<sub>2</sub> Hybrid Nano-Architectures with Abundant Active Edge Sites for High-Rate Asymmetric Supercapacitors and Hydrogen Evolution Reactions. *Small* **2023**, *19*, 2205881. [[CrossRef](#)]
88. Zhang, Y.; Chen, X.; Huang, Y.; Zhang, C.; Li, F.; Shu, H. The Role of Intrinsic Defects in Electrocatalytic Activity of Monolayer VS<sub>2</sub> Basal Planes for the Hydrogen Evolution Reaction. *J. Phys. Chem. C* **2017**, *121*, 1530–1536. [[CrossRef](#)]



89. Wang, L.; Gao, W.; Chen, X.; Liu, Y.; Qureshi, A.H.; Liu, Y.; Chen, M.; Zhang, X.; Guo, Y.; Wang, J. Charge-Modulated VS<sub>2</sub> Monolayer for Effective Hydrogen Evolution Reaction. *J. Phys. Chem. C* **2021**, *125*, 12004–12011. [[CrossRef](#)]
90. Zhang, J.; Zhang, C.; Wang, Z.; Zhu, J.; Wen, Z.; Zhao, X.; Zhang, X.; Xu, J.; Lu, Z. Synergistic Interlayer and Defect Engineering in VS<sub>2</sub> Nanosheets toward Efficient Electrocatalytic Hydrogen Evolution Reaction. *Small* **2018**, *14*, 1703098. [[CrossRef](#)]
91. Xu, J.; Zhu, Y.; Yu, B.; Fang, C.; Zhang, J. Metallic 1T-VS<sub>2</sub> nanosheets featuring V<sup>2+</sup> self-doping and mesopores towards an efficient hydrogen evolution reaction. *Inorg. Chem. Front.* **2019**, *6*, 3510–3517. [[CrossRef](#)]
92. Singh, V.K.; Nakate, U.T.; Bhuyan, P.; Chen, J.; Tran, D.T.; Park, S. Mo/Co doped 1T-VS<sub>2</sub> nanostructures as a superior bifunctional electrocatalyst for overall water splitting in alkaline media. *J. Mater. Chem. A* **2022**, *10*, 9067–9079. [[CrossRef](#)]
93. He, W.; Zheng, X.; Peng, J.; Dong, H.; Wang, J.; Zhao, W. Mo-dopant-strengthened basal-plane activity in VS<sub>2</sub> for accelerating hydrogen evolution reaction. *Chem. Eng. J.* **2020**, *396*, 125227. [[CrossRef](#)]
94. Mohan, P.; Yang, J.; Jena, A.; Suk Shin, H. VS<sub>2</sub>/rGO hybrid nanosheets prepared by annealing of VS<sub>4</sub>/rGO. *J. Solid State Chem.* **2015**, *224*, 82–87. [[CrossRef](#)]
95. Patil, S.A.; Rabani, I.; Hussain, S.; Seo, Y.-S.; Jung, J.; Shrestha, N.K.; Im, H.; Kim, H. A Facile Design of Solution-Phase Based VS<sub>2</sub> Multifunctional Electrode for Green Energy Harvesting and Storage. *Nanomaterials* **2022**, *12*, 339. [[CrossRef](#)]
96. Du, C.; Liang, D.; Shang, M.; Zhang, J.; Mao, J.; Liu, P.; Song, W. In Situ Engineering MoS<sub>2</sub> NDs/VSe<sub>2</sub> Lamellar Heterostructure for Enhanced Electrocatalytic Hydrogen Evolution. *ACS Sustain. Chem. Eng.* **2018**, *6*, 15471–15479. [[CrossRef](#)]
97. Hou, Z.; Cui, C.; Yang, Y.; Zhang, T. Electrochemical Oxidation Encapsulated Ru Clusters Enable Robust Durability for Efficient Oxygen Evolution. *Small* **2023**, *19*, 2207170. [[CrossRef](#)]
98. Zhong, X.; Tang, J.; Wang, J.; Shao, M.; Chai, J.; Wang, S.; Yang, M.; Yang, Y.; Wang, N.; Wang, S.; et al. 3D heterostructured pure and N-Doped Ni<sub>3</sub>S<sub>2</sub>/VS<sub>2</sub> nanosheets for high efficient overall water splitting. *Electrochim. Acta* **2018**, *269*, 55–61. [[CrossRef](#)]
99. Kwak, I.H.; Kim, J.Y.; Zewdie, G.M.; Yang, J.; Lee, K.-S.; Yoo, S.J.; Kwon, I.S.; Park, J.; Kang, H.S. Electrocatalytic Activation in ReSe<sub>2</sub>-VSe<sub>2</sub> Alloy Nanosheets to Boost Water-Splitting Hydrogen Evolution Reaction. *Adv. Mater.* **2024**, *36*, 2310769. [[CrossRef](#)]
100. Pan, U.N.; Kandel, M.R.; Tomar, A.K.; Kim, N.H.; Lee, J.H. Synchronous Surface-Interface and Crystal-Phase Engineered Multifaceted Hybrid Nanostructure of Fe-(1T)-VSe<sub>2</sub> Nanosheet and Fe-CoSe<sub>2</sub> Nanorods Doped with P for Rapid HER and OER, Kinetics. *Small* **2024**, *20*, 2305519. [[CrossRef](#)]
101. Samal, R.; Shinde, P.V.; Rout, C.S. 2D Vanadium diselenide supported on reduced graphene oxide for water electrolysis: A comprehensive study in alkaline media. *Emergent Mater.* **2021**, *4*, 1047–1053. [[CrossRef](#)]
102. Tomar, S.; Sen, P.; Chakraborty, S. Single atom functionalization in vanadium dichalcogenide monolayers: Towards enhanced electrocatalytic activity. *Sustain. Energy Fuels* **2022**, *6*, 5337–5344. [[CrossRef](#)]
103. Qin, Z.; Wang, Z.; Zhao, J. Computational screening of single-atom catalysts supported by VS<sub>2</sub> monolayers for electrocatalytic oxygen reduction/evolution reactions. *Nanoscale* **2022**, *14*, 6902–6911. [[CrossRef](#)]
104. Dhakal, P.P.; Pan, U.N.; Paudel, D.R.; Kandel, M.R.; Kim, N.H.; Lee, J.H. Cobalt–manganese sulfide hybridized Fe-doped 1T-Vanadium disulfide 3D-Hierarchical core-shell nanorods for extreme low potential overall water-splitting. *Mater. Today Nano* **2022**, *20*, 100272. [[CrossRef](#)]
105. Zhang, Z.; Yang, P.; Hong, M.; Jiang, S.; Zhao, G.; Shi, J.; Xie, Q.; Zhang, Y. Recent progress in the controlled synthesis of 2D metallic transition metal dichalcogenides. *Nanotechnology* **2019**, *30*, 182002. [[CrossRef](#)]
106. Tsai, C.; Chan, K.; Nørskov, J.K.; Abild-Pedersen, F. Theoretical insights into the hydrogen evolution activity of layered transition metal dichalcogenides. *Surf. Sci.* **2015**, *640*, 133–140. [[CrossRef](#)]
107. Li, D.; Wang, X.; Kan, C.-m.; He, D.; Li, Z.; Hao, Q.; Zhao, H.; Wu, C.; Jin, C.; Cui, X. Structural Phase Transition of Multilayer VSe<sub>2</sub>. *ACS Appl. Mater. Interfaces* **2020**, *12*, 25143–25149. [[CrossRef](#)]
108. Zhao, W.; Dong, B.; Guo, Z.; Su, G.; Gao, R.; Wang, W.; Cao, L. Colloidal synthesis of VSe<sub>2</sub> single-layer nanosheets as novel electrocatalysts for the hydrogen evolution reaction. *Chem. Commun.* **2016**, *52*, 9228–9231. [[CrossRef](#)]
109. Fu, J.; Ali, R.; Mu, C.; Liu, Y.; Mahmood, N.; Lau, W.-M.; Jian, X. Large-scale preparation of 2D VSe<sub>2</sub> through a defect-engineering approach for efficient hydrogen evolution reaction. *Chem. Eng. J.* **2021**, *411*, 128494. [[CrossRef](#)]
110. Wang, R.; Guo, Z.; Tan, X.; Zhang, J.; Yang, L.; Wang, W.; Cao, L.; Dong, B. Atmosphere plasma treatment and Co heteroatoms doping on basal plane of colloidal 2D VSe<sub>2</sub> nanosheets for enhanced hydrogen evolution. *Int. J. Hydrogen Energy* **2021**, *46*, 32425–32434. [[CrossRef](#)]
111. Kuniyil, N.; Koottumvathukkal Anil Raj, S.R.; Rout, C.S. Selective Growth of Molybdenum Sulfo-Selenides on a Defect-Rich Carbon Nanotube Skeleton for Efficient Energy Storage and Hydrogen Generation Applications. *Energy Fuels* **2022**, *36*, 13346–13355. [[CrossRef](#)]
112. Zhang, J.; Li, J.; Huang, H.; Chen, W.; Cui, Y.; Li, Y.; Mao, W.; Zhu, X.; Li, X.a. Spatial Relation Controllable Di-Defects Synergy Boosts Electrocatalytic Hydrogen Evolution Reaction over VSe<sub>2</sub> Nanoflakes in All pH Electrolytes. *Small* **2022**, *18*, 2204557. [[CrossRef](#)]
113. Wang, C.; Jin, M.; Liu, D.; Liang, F.; Luo, C.; Li, P.; Cai, C.; Bi, H.; Wu, X.; Di, Z. VSe<sub>2</sub> quantum dots with high-density active edges for flexible efficient hydrogen evolution reaction. *J. Phys. D Appl. Phys.* **2021**, *54*, 214006. [[CrossRef](#)]
114. Hu, L.-Y.; Yu, L.-F.; Yang, H.; Xu, X.; Wang, F.; Xu, X.-H. Room-temperature ferromagnetism enhancement in Fe-doped VSe<sub>2</sub> nanosheets synthesized by a chemical method. *Rare Met.* **2021**, *40*, 2501–2507. [[CrossRef](#)]
115. Xiong, Z.; Hu, C.; Luo, X.; Zhou, W.; Jiang, Z.; Yang, Y.; Yu, T.; Lei, W.; Yuan, C. Field-Free Improvement of Oxygen Evolution Reaction in Magnetic Two-Dimensional Heterostructures. *Nano Lett.* **2021**, *21*, 10486–10493. [[CrossRef](#)]

116. Sun, Y.; Sun, S.; Yang, H.; Xi, S.; Gracia, J.; Xu, Z.J. Spin-Related Electron Transfer and Orbital Interactions in Oxygen Electrocatalysis. *Adv. Mater.* **2020**, *32*, 2003297. [[CrossRef](#)]
117. Chen, M.; Zhou, W.; Ye, K.; Yuan, C.; Zhu, M.; Yu, H.; Yang, H.; Huang, H.; Wu, Y.; Zhang, J.; et al. External Fields Assisted Highly Efficient Oxygen Evolution Reaction of Confined 1T-VSe<sub>2</sub> Ferromagnetic Nanoparticles. *Small* **2023**, *19*, 2300122. [[CrossRef](#)]
118. Zheng, J.; Zhang, W.; Zhang, J.; Lv, M.; Li, S.; Song, H.; Cui, Z.; Du, L.; Liao, S. Recent advances in nanostructured transition metal nitrides for fuel cells. *J. Mater. Chem. A* **2020**, *8*, 20803–20818. [[CrossRef](#)]
119. Chen, P.; Ye, J.; Wang, H.; Ouyang, L.; Zhu, M. Recent progress of transition metal carbides/nitrides for electrocatalytic water splitting. *J. Alloys Compd.* **2021**, *883*, 160833. [[CrossRef](#)]
120. Fu, C.; Feng, L.; Yin, H.; Li, Y.; Li, G.; Feng, Y.; Cao, L.; Huang, J.; Liu, Y. Synergistic Coupling of Hierarchical Heterostructured Ni<sub>3</sub>P/Ni/VN Microflower Electrocatalyst for Enhanced Hydrogen Evolution Reaction. *ChemCatChem* **2023**, *15*, e202201399. [[CrossRef](#)]
121. He, X.; Tian, Y.; Deng, D.; Chen, F.; Wu, J.; Qian, J.; Li, H.; Xu, L. Engineering Antiperovskite Ni<sub>4</sub>N/VN Heterostructure with Improved Intrinsic Interfacial Charge Transfer as a Bifunctional Catalyst for Rechargeable Zinc–Air Batteries. *ACS Sustain. Chem. Eng.* **2021**, *9*, 17007–17015. [[CrossRef](#)]
122. Meng, K.; Wen, S.; Liu, L.; Jia, Z.; Wang, Y.; Shao, Z.; Qi, T. Vertically Grown MoS<sub>2</sub> Nanoplates on VN with an Enlarged Surface Area as an Efficient and Stable Electrocatalyst for HER. *ACS Appl. Energy Mater.* **2019**, *2*, 2854–2861. [[CrossRef](#)]
123. Zhou, P.; Xing, D.; Liu, Y.; Wang, Z.; Wang, P.; Zheng, Z.; Qin, X.; Zhang, X.; Dai, Y.; Huang, B. Accelerated electrocatalytic hydrogen evolution on non-noble metal containing trinickel nitride by introduction of vanadium nitride. *J. Mater. Chem. A* **2019**, *7*, 5513–5521. [[CrossRef](#)]
124. Yu, X.; Cheng, F.; Xie, K. Porous single-crystalline vanadium nitride octahedra with a unique electrocatalytic performance. *New J. Chem.* **2022**, *46*, 1392–1398. [[CrossRef](#)]
125. Feng, J.; Tang, R.; Liu, G.; Meng, T. Regulating d-orbital electronic character and HER free energy of VN electrocatalyst by anchoring single atom. *Chem. Eng. J.* **2023**, *452*, 139131. [[CrossRef](#)]
126. Liu, Q.; Liu, K.; Li, X.; Hui, C.; Huang, J.; Deng, Z.; Yang, D.; Cao, L.; Feng, L. Ni and VN Nanoparticles Supported on N-Doped Carbon Layer Containing Ni Single Atoms as Electrocatalyst for the Hydrogen Evolution Reaction. *ACS Appl. Nano Mater.* **2024**, *7*, 4059–4067. [[CrossRef](#)]
127. Pi, C.; Zhao, Z.; Zhang, X.; Gao, B.; Zheng, Y.; Chu, P.K.; Yang, L.; Huo, K. In situ construction of  $\gamma$ -MoC/VN heterostructured electrocatalysts with strong electron coupling for highly efficient hydrogen evolution reaction. *Chem. Eng. J.* **2021**, *416*, 129130. [[CrossRef](#)]
128. Li, Q.; Yang, P.; Liu, Y.; Xiao, W.; Xiao, Z.; Xu, G.; Wang, L.; Liu, F.; Wu, Z. In-situ construction of pomegranate-like nickel-vanadium nitride for hydrogen production through urea-assisted water-splitting. *J. Alloys Compd.* **2023**, *968*, 171861. [[CrossRef](#)]
129. Meng, K.; Zheng, Z.; Cao, J.; Liu, L.; Jia, Z.; Wang, Y.; Qi, T. Vanadium nitride based CoFe prussian blue analogues for enhanced electrocatalytic oxygen evolution. *Int. J. Hydrogen Energy* **2020**, *45*, 31410–31417. [[CrossRef](#)]
130. Li, X.; Huang, J.; Feng, L.; He, D.; Liu, Z.; Li, G.; Zhang, N.; Feng, Y.; Cao, L. Molybdenum and cobalt co-doped VC nanoparticles encapsulated in nanocarbon as efficient electrocatalysts for the hydrogen evolution reaction. *Inorg. Chem. Front.* **2022**, *9*, 870–878. [[CrossRef](#)]
131. Zheng, Y.; Mou, Y.; Wang, Y.; Wan, J.; Yao, G.; Feng, C.; Sun, Y.; Dai, L.; Zhang, H.; Wang, Y. Aluminum-incorporation activates vanadium carbide with electron-rich carbon sites for efficient pH-universal hydrogen evolution reaction. *J. Colloid Interface Sci.* **2024**, *656*, 367–375. [[CrossRef](#)]
132. Peng, X.; Huang, C.; Zhang, B.; Liu, Y. Vanadium carbide nanodots anchored on N doped carbon nanosheets fabricated by spatially confined synthesis as a high-efficient electrocatalyst for hydrogen evolution reaction. *J. Power Sources* **2021**, *490*, 229551. [[CrossRef](#)]
133. Wu, L.; Zhang, M.; Wen, Z.; Ci, S. V<sub>8</sub>C<sub>7</sub> decorating CoP nanosheets-assembled microspheres as trifunctional catalysts toward energy-saving electrolytic hydrogen production. *Chem. Eng. J.* **2020**, *399*, 125728. [[CrossRef](#)]
134. Suo, N.; Han, X.; Chen, C.; He, X.; Dou, Z.; Lin, Z.; Cui, L.; Xiang, J. Engineering vanadium phosphide by iron doping as bifunctional electrocatalyst for overall water splitting. *Electrochim. Acta* **2020**, *333*, 135531. [[CrossRef](#)]
135. Han, H.; Yi, F.; Choi, S.; Kim, J.; Kwon, J.; Park, K.; Song, T. Self-supported vanadium-incorporated cobalt phosphide as a highly efficient bifunctional electrocatalyst for water splitting. *J. Alloys Compd.* **2020**, *846*, 156350. [[CrossRef](#)]
136. Zhu, R.; Chen, F.; Wang, J.; Song, Y.; Cheng, J.; Mao, M.; Ma, H.; Lu, J.; Cheng, Y. Multi-channel V-doped CoP hollow nanofibers as high-performance hydrogen evolution reaction electrocatalysts. *Nanoscale* **2020**, *12*, 9144–9151. [[CrossRef](#)]
137. Zhu, Z.; Xu, K.; Guo, W.; Zhang, H.; Xiao, X.; He, M.; Yu, T.; Zhao, H.; Zhang, D.; Yang, T. Vanadium-phosphorus incorporation induced interfacial modification on cobalt catalyst and its super electrocatalysis for water splitting in alkaline media. *Appl. Catal. B* **2022**, *304*, 120985. [[CrossRef](#)]
138. Yang, H.; Hu, Y.; Huang, D.; Xiong, T.; Li, M.; Balogun, M.S.; Tong, Y. Efficient hydrogen and oxygen evolution electrocatalysis by cobalt and phosphorus dual-doped vanadium nitride nanowires. *Mater. Today Chem.* **2019**, *11*, 1–7. [[CrossRef](#)]
139. Peng, L.; Shen, J.; Zhang, L.; Wang, Y.; Xiang, R.; Li, J.; Li, L.; Wei, Z. Graphitized carbon-coated vanadium carbide nanoboscajes modified by nickel with enhanced electrocatalytic activity for hydrogen evolution in both acid and alkaline solutions. *J. Mater. Chem. A* **2017**, *5*, 23028–23034. [[CrossRef](#)]

140. Ma, W.; Wan, J.; Fu, W.; Wu, Y.; Wang, Y.; Zhang, H.; Wang, Y. Heterostructures induced between platinum nanoparticles and vanadium carbide boosting hydrogen evolution reaction. *Appl. Catal. A* **2022**, *633*, 118512. [[CrossRef](#)]
141. Cao, L.; Zhang, N.; Feng, L.; Huang, J.; Feng, Y.; Li, W.; Yang, D.; Liu, Q. Well-dispersed ultrasmall VC nanoparticles embedded in N-doped carbon nanotubes as highly efficient electrocatalysts for hydrogen evolution reaction. *Nanoscale* **2018**, *10*, 14272–14279. [[CrossRef](#)]
142. Wan, J.; Wang, C.; Tang, Q.; Gu, X.; He, M. First-principles study of vanadium carbides as electrocatalysts for hydrogen and oxygen evolution reactions. *RSC Adv.* **2019**, *9*, 37467–37473. [[CrossRef](#)]
143. Kawashima, K.; Cao, C.L.; Li, H.; Márquez-Montes, R.A.; Wygant, B.R.; Son, Y.J.; Guerrero, J.V.; Henkelman, G.; Mullins, C.B. Evaluation of a  $V_8C_7$  Anode for Oxygen Evolution in Alkaline Media: Unusual Morphological Behavior. *ACS Sustain. Chem. Eng.* **2020**, *8*, 14101–14108. [[CrossRef](#)]
144. Pu, Z.; Liu, T.; Amiin, I.S.; Cheng, R.; Wang, P.; Zhang, C.; Ji, P.; Hu, W.; Liu, J.; Mu, S. Transition-Metal Phosphides: Activity Origin, Energy-Related Electrocatalysis Applications, and Synthetic Strategies. *Adv. Funct. Mater.* **2020**, *30*, 2004009. [[CrossRef](#)]
145. Anne Acedera, R.; Therese Dumlao, A.; Donn Matienzo, D.J.; Divinagracia, M.; Anne Paraggua, J.; Abel Chuang, P.-Y.; Ocon, J. Templated synthesis of transition metal phosphide electrocatalysts for oxygen and hydrogen evolution reactions. *J. Energy Chem.* **2024**, *89*, 646–669. [[CrossRef](#)]
146. Theerthagiri, J.; Murthy, A.P.; Lee, S.J.; Karuppusamy, K.; Arumugam, S.R.; Yu, Y.; Hanafiah, M.M.; Kim, H.-S.; Mittal, V.; Choi, M.Y. Recent progress on synthetic strategies and applications of transition metal phosphides in energy storage and conversion. *Ceram. Int.* **2021**, *47*, 4404–4425. [[CrossRef](#)]
147. Zhang, W.; Han, N.; Luo, J.; Han, X.; Feng, S.; Guo, W.; Xie, S.; Zhou, Z.; Subramanian, P.; Wan, K.; et al. Critical Role of Phosphorus in Hollow Structures Cobalt-Based Phosphides as Bifunctional Catalysts for Water Splitting. *Small* **2022**, *18*, 2103561. [[CrossRef](#)]
148. Mo, Y.; Ni, Y.; Li, X.; Pan, R.; Tang, Y.; Deng, Y.; Xiao, B.; Tan, Y.; Fang, Y. An efficient pH-universal non-noble hydrogen-evolving electrocatalyst from transition metal phosphides-based heterostructures. *Int. J. Hydrogen Energy* **2023**, *48*, 31101–31109. [[CrossRef](#)]
149. Wang, C.; Wang, Q.; Du, X.; Zhang, X.; Hu, T. Controlled synthesis of CoVP as robust electrocatalysts for water, seawater and urea oxidation. *Int. J. Hydrogen Energy* **2023**, *48*, 34370–34381. [[CrossRef](#)]

**Disclaimer/Publisher’s Note:** The statements, opinions and data contained in all publications are solely those of the individual author(s) and contributor(s) and not of MDPI and/or the editor(s). MDPI and/or the editor(s) disclaim responsibility for any injury to people or property resulting from any ideas, methods, instructions or products referred to in the content.